© 2016. Published by The Company of Biologists Ltd | Development (2016) 143, 1108-1119 doi:10.1242/dev.127365

The Myb-domain protein ULTRAPETALA1 INTERACTING FACTOR 1 controls floral meristem activities in *Arabidopsis*

Fanny Moreau[1,2,3,4], Emmanuel Thévenon[1,2,3,4], Robert Blanvillain[1,2,3,4], Irene Lopez-Vidriero[5], Jose Manuel Franco-Zorrilla[5], Renaud Dumas[1,2,3,4], François Parcy[1,2,3,4], Patrice Morel[6], Christophe Trehin[6] and Cristel C. Carles[1,2,3,4,*]

ABSTRACT

Higher plants continuously and iteratively produce new above-ground organs in the form of leaves, stems and flowers. These organs arise from shoot apical meristems whose homeostasis depends on coordination between self-renewal of stem cells and their differentiation into organ founder cells. This coordination is stringently controlled by the central transcription factor WUSCHEL (WUS), which is both necessary and sufficient for stem cell specification in *Arabidopsis thaliana*. ULTRAPETALA1 (ULT1) was previously identified as a plant-specific, negative regulator of *WUS* expression. However, molecular mechanisms underlying this regulation remain unknown. ULT1 protein contains a SAND putative DNA-binding domain and a B-box, previously proposed as a protein interaction domain in eukaryotes. Here, we characterise a novel partner of ULT1, named ULT1 INTERACTING FACTOR 1 (UIF1), which contains a Myb domain and an EAR motif. UIF1 and ULT1 function in the same pathway for regulation of organ number in the flower. Moreover, UIF1 displays DNA-binding activity and specifically binds to *WUS* regulatory elements. We thus provide genetic and molecular evidence that UIF1 and ULT1 work together in floral meristem homeostasis, probably by direct repression of *WUS* expression.

KEY WORDS: *Arabidopsis thaliana*, Stem cell, Flower, WUSCHEL, Myb transcription factor, Repressor

INTRODUCTION

Plants differ from the majority of animals by their ability to produce new organs throughout their life cycle. Continuous organogenesis is allowed by the maintenance of stem cell reservoirs sustained through continuous cell divisions in dynamic structures called meristems (Carles and Fletcher, 2003; Holt et al., 2014; Gaillochet et al., 2015). The shoot apical meristem (SAM) is located at the growing apex and produces cells that will be incorporated into new structures such as lateral organs. Cell divisions constantly replenish the meristem in its central zone (CZ), thus providing a cell reservoir for the adjacent peripheral zone (PZ). PZ cells further differentiate into lateral organ primordia on the meristem flanks (Irish and Sussex, 1992; Leyser and Furner, 1992). Proper, continuous growth of the plant thus requires long-term function of the SAM, itself depending on a coordinated balance between cell proliferation and differentiation (Laux, 2003; Ha et al., 2010).

In *Arabidopsis thaliana*, SAM homeostasis is governed by a feedback loop signalling network involving the CLAVATA (CLV) and WUSCHEL (WUS) factors (Ha et al., 2010). The WUS homeobox transcription factor is both necessary and sufficient for stem cell specification (Laux et al., 1996; Mayer et al., 1998; Schoof et al., 2000; Lenhard et al., 2002; Gallois et al., 2004; Leibfried et al., 2005). In mutants with defective WUS function, the activity of the SAM stops at early stages of development, correlating with a lack of stem cells. *WUS* is expressed in a small central meristematic zone called the organizing centre (OC). The WUS protein, after being synthesised in cells of the OC, migrates in the adjacent cells of the CZ where it promotes stem-cell identity and both directly and indirectly regulates transcription of the CLV genes (Busch et al., 2010; Yadav et al., 2011; Schuster et al., 2014). In turn, the CLV3 signalling peptide restricts *WUS* expression to the OC (Mayer et al., 1998; Brand et al., 2000), via the CLV1-CLV2-CRN receptor protein complexes and the RPK2 receptor-like kinase (Fletcher et al., 1999; Rojo et al., 2002; Lenhard and Laux, 2003; Müller et al., 2008; Ogawa et al., 2008; Wang and Fiers, 2010; Kinoshita et al., 2010). As a consequence, *clv* loss-of-function mutants produce a widely enlarged SAM and more lateral organs, owing to extreme expansion of the *WUS* expression domain (Clark et al., 1993; Schoof et al., 2000). Thus, the WUS-CLV negative feedback loop is crucial for the maintenance of meristem size and function.

During the vegetative stage, the SAM produces leaves and axillary meristems that reiterate SAM development, whereas during the reproductive stage, SAM and axillary meristems produce flower meristems (FMs), which develop into flowers (Alvarez-Buylla et al., 2010). In *A. thaliana*, flowers are made of four whorls, or concentric rings, each carrying a fixed number of organs with distinct identities: four sepals, four petals, six stamens and two fused carpels. Stem cell activity at the FM determines the number of organs carried by each whorl and is regulated by the same WUS-CLV feedback loop, as flowers of *clv* mutants produce more organs per whorl, whereas *wus* hypomorphic mutants produce fewer floral organs than do wild-type (WT) plants (Laux et al., 1996; Schoof et al., 2000). Moreover and in contrast to the SAM, FM growth is determinate as organ production ceases once the carpels are initiated in the innermost whorl of the flower (Prunet et al., 2009). FM termination relies on the timely expression of the flower homeotic gene *AGAMOUS* (*AG*), which encodes a MADS domain-containing protein that both directly and indirectly represses *WUS* expression in the centre of the FM, leading to extinction of stem cell activity at stage 6 (Lenhard et al., 2001; Lohmann et al., 2001; Sun et al., 2009, 2014; Liu et al., 2011).

[1]Université Grenoble Alpes, Laboratoire de Physiologie Cellulaire et Végétale (LPCV), Grenoble 38054, France. [2]CNRS, LPCV, UMR 5168, Grenoble 38054, France. [3]CEA, Direction des Sciences du Vivant, BIG, LPCV, Grenoble 38054, France. [4]INRA, LPCV, Grenoble 38054, France. [5]Genomics Unit, Centro Nacional de Biotecnologia CNB- CSIC, Darwin 3, Madrid 28049, Spain. [6]Laboratoire de Reproduction et Développement des Plantes, Université Lyon1, CNRS, INRA, ENS, Lyon cedex 07 69347, France.

*Author for correspondence (Christel.carles@ujf-grenoble.fr)

Received 16 June 2015; Accepted 15 February 2016

Development (2016) 143, 1108-1119 doi:10.1242/dev.127365

The *A. thaliana* ULTRAPETALA1 (ULT1) factor is a key negative regulator of stem cell activity in the shoot apical and floral meristems (Fletcher, 2001; Carles et al., 2004, 2005). In particular, *ult1* loss-of-function mutants produce more flowers and supernumerary floral organs of each type. In these mutants, the inflorescence and flower meristem sizes are enlarged as a result of the expansion of the *WUS* expression domain (Carles et al., 2004, 2005). Thus, ULT1 maintains shoot and floral meristem function by restricting *WUS* expression to the OC. Moreover, FM termination is delayed in *ult1* mutants (Fletcher, 2001; Prunet et al., 2008), leading to the production of additional organs inside the innermost whorl, such as stamens and carpelloid structures. This phenotype correlates with a delay in *AG* induction, which, in turn, delays *WUS* extinction in the centre of the FM (Fletcher, 2001; Carles et al., 2004). Thus, ULT1 acts as a negative regulator of *WUS* expression in the FM, and this function is required for both meristem homeostasis and termination (Carles et al., 2004). The *ULT1* gene encodes a plant-specific protein composed of a SAND (Sp100, AIRE-1, NucP41/75 and DEAF-1) putative DNA-interacting domain and a B-box, which is likely to be involved in protein-protein interaction (Carles et al., 2005). It has been proposed that ULT1 directly activates *AG* at the centre of the FM, via interaction with the chromatin activator ARABIDOPSIS HOMOLOG OF TRITHORAX 1 (ATX1) (Alvarez-Venegas et al., 2003; Ding et al., 2011), leading to a reduction in trimethyl marks at lysine 27 of histone 3 (H3K27me3, repressive chromatin mark) at the target locus (Carles and Fletcher, 2009, 2010; Engelhorn et al., 2014a). Thus, ULT1 acts as a positive regulator of *AG* that contributes to the extinction of *WUS* expression in stage 8 flowers.

However, several questions remain open concerning the precise molecular mechanism(s) through which ULT1 regulates flower meristem activity. How does ULT1 repress *WUS* for SAM and FM homeostasis at early stages of flower development? Could ULT1 directly function in *WUS* repression? How does ULT1 interact with DNA and what defines its target gene specificity? In order to elucidate the answers to these questions, we searched for novel ULT1 interacting partners. Here, we identify and characterise ULT1 INTERACTING FACTOR 1 (UIF1), a Myb domain-containing transcription factor. We found that loss of function in *UIF1* causes phenotypes similar to *ult1* mutant phenotypes, such as production of supernumerary floral organs. We show that *UIF1* and *ULT1* function in the same pathway for the regulation of organ number in the flower. Moreover, UIF1 displays DNA-binding activity and specifically binds to *WUS* regulatory elements. Because UIF1 protein displays a transcriptional repressor activity, we propose that UIF1 and ULT1 work together in FM homeostasis, via direct regulation of *WUS* expression.

RESULTS

The Myb domain-containing protein UIF1 interacts with ULT1

To identify novel interactors of ULT1, we performed a yeast two-hybrid (Y2H) screen, using an *A. thaliana* inflorescence and flower cDNA library and the full-length ULT1 open reading frame (ORF) as bait. Upon selection, we isolated a clone corresponding to *At4g37180.1* as annotated in the tair database (https://www.arabidopsis.org/servlets/TairObject?id=126622&type=locus), which we named *ULT1 INTERACTING FACTOR 1* (*UIF1*) (Fig. 1A). A targeted binary Y2H test using the full-length ULT1 and UIF1 proteins confirmed the interaction (Fig. 1B; Fig. S1A). The UIF1-ULT1 interaction was next validated *in planta* by a bimolecular fluorescence complementation (BiFC) assay, yielding an interaction signal in the nucleus of transformed cells (Fig. 1C; Fig. S1B). The 1804-bp long *UIF1* gene (*At4g37180*) encodes a 356-aa long Myb domain-containing protein of unreported function, belonging to the GARP G2-like subfamily of transcription factors (Fig. 2A,B). The Myb-like putative DNA-binding domain of UIF1 (aa 209-268) contains a SHLQKYR motif at its C-terminus (Fig. 2B); this motif is found in other plant proteins (At*CCA1*; At*LHY*; *LeMYB1*; *ZmMRP-1*; *MybSt1*) and reported as a specific DNA-binding domain (Wang et al., 1997; Schaffer et al., 1998; Rose et al., 1999; Gómez et al., 2002; Baranowskij et al., 1994). UIF1 protein also contains two distinct EAR-like motifs (LxLxL, with L indicating leucine and x indicating any aa) at its N- and C-terminal ends, as well as a predicted nuclear localisation signal (NLS) (Hiratsu et al., 2002; Ohta et al., 2001) (Fig. 2B). We found six homologues for UIF1 in *A. thaliana* (Fig. S2A,B), which share 86-91% similarity over their Myb domain and 43-63% similarity over the full-length protein. Another globular domain rich in hydrophobic amino acids (aa 45-86) such as L and isoleucine (I) shows 78-81% similarity between all homologues (Fig. S2A). We identified orthologues of UIF1 among monocots and dicots (Fig. 2B), which share strong similarity both over the hydrophobic and Myb domains (68-83% and 88-96%, respectively). Interestingly, although the N-terminal EAR motif is conserved among all UIF1 orthologues, UIF1 differs by the presence of an additional LDLEL EAR-like motif at its C-terminus end (Fig. 2B). Phylogenetic reconstructions generated with *UIF1* orthologues in eudicots suggest that, unlike At1*g*13300 and At3*g*25790 on one hand, and At1*g*68670 and At1*g*25550 on the other hand, the *UIF1* gene does not result from duplication in the Brassicaceae lineage (Fig. S2C).

In order to map the regions necessary for ULT1-UIF1 interaction, we tested truncated versions of ULT1 and UIF1 by Y2H and BiFC (Fig. 1A,C). We showed that in the absence of the B-box domain (Carles et al., 2005), ULT1 (ULT1 1-193) does not interact with UIF1 in Y2H (Fig. 1B) or in BiFC (Fig. 1C). Furthermore, the ULT1 B-box domain alone (aa 116-237) could interact with UIF1 and restore yeast growth on selective medium (Fig. 1A,B). Similarly, we showed that deletion of the N-terminal domain of UIF1 (UIF1 93-364), which contains the (L/I)-rich motif, resulted in the loss of interaction with ULT1 (Fig. 1A,C). Taken together, these results suggest that UIF1 can interact with the ULT1 protein and that ULT1 B-box and UIF1 N-terminus are required for this interaction.

UIF1 and *ULT1* display overlapping expression patterns in inflorescences

To investigate the functional significance of UIF1-ULT1 interaction, we analysed the temporal and spatial expression pattern of *UIF1* in *A. thaliana* WT tissues. Quantitative real-time RT-PCR (RT-qPCR) analysis showed that *UIF1* is expressed in all tested tissues: roots, 6-day-old (do) seedlings, inflorescences, closed flowers and open flowers, with highest levels in 6-do seedlings and inflorescences (Fig. 2C). This profile is similar to that of *ULT1* and was confirmed by microarray data grouped in the public eFP Browser database (http://bbc.botany.utoronto.ca/efp/cgi-bin/efpWeb.cgi; Fig. S3A). In particular, *ULT1* and *UIF1* expression patterns overlap in vegetative shoot apex, floral buds and floral organs especially in stamens and carpels (in stage 12-15 flowers). At the cellular level, RNA *in situ* hybridisation experiments on inflorescence and flower tissue sections (Fig. 2D-F; Fig. S3B,C) showed that *UIF1* is expressed throughout the inflorescence meristem (Fig. 2D) and in floral primordia from stage 2 onwards, being restricted later to stamens and to the adaxial side of carpel primordia (Fig. 2E). In mature flowers, *UIF1* transcripts were also found in ovules (Fig. 2F). This pattern largely overlaps with that of

Development (2016) 143, 1108-1119 doi:10.1242/dev.127365

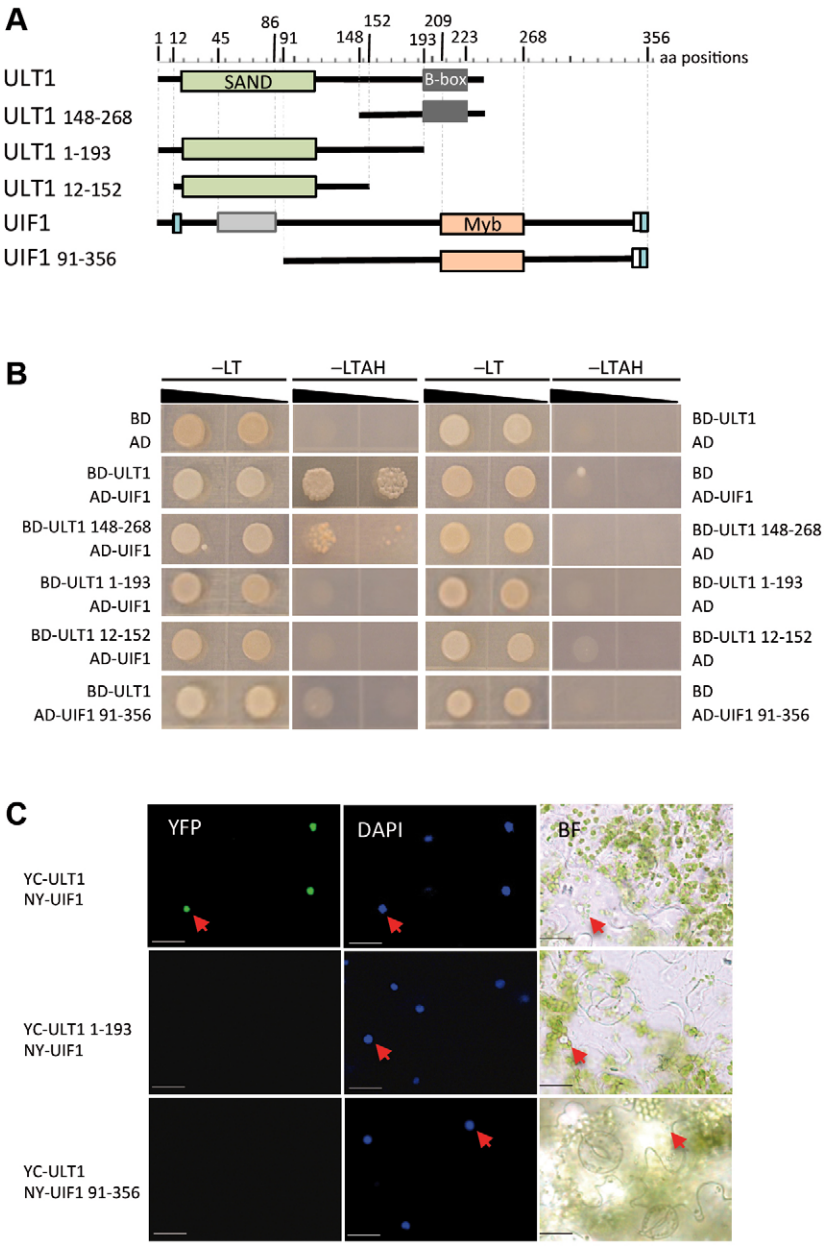

Fig. 1. ULT1 interacts with the UIF1 Myb domain-containing protein *in vivo*. (A) Diagram of ULT1 and UIF1 full length or truncated versions used in interaction studies. ULT1: SAND domain (green box), B-box like domain (dark grey box). UIF1: hydrophobic domain (light grey box), Myb domain (orange box), predicted NLS (white box), EAR-like motifs (blue boxes). (B) ULT1 interacts with UIF1 in Y2H assays. The truncated version of ULT1 carrying the B-box domain (ULT1 148-268) shows some interaction with UIF1, whereas the truncated versions lacking the B-box domain (ULT1 1-193 and ULT1 12-152) do not show any interaction. The truncated version of UIF1 lacking the N-terminus portion (UIF1 91-356) does not show interaction with ULT1. Yeast strains were dotted on –LT or –LTAH medium (on which only protein interaction allows growth). ULT1-ULT1 interaction: positive control; empty vectors: negative controls. BD, DNA-binding domain, AD, activation domain. (C) ULT1 and UIF1 interact in the nucleus of tobacco cells in BiFC experiments. The truncated ULT1 1-193 protein does not show interaction with UIF1 and the truncated UIF1 91-356 does not show interaction with ULT1. This indicates that the C-terminus of ULT1 containing the B-box domain and the N-terminus of UIF1 are required for interaction between the two proteins. From left to right, green channel (YFP filter), blue channel (DAPI filter) and bright field (BF). Red arrows indicate cell nuclei. Scale bars: 2 µm.

ULT1 transcripts (Carles et al., 2005). Finally, at the subcellular level, we found that the GFP-UIF1 fusion protein localises in the nucleus and in cytosolic foci in the cell (Fig. 2G), a pattern very similar to that reported for the ULT1 protein (Carles et al., 2005).

Altogether, similarities in expression patterns and protein subcellular localisation further support a molecular interaction for ULT1 and UIF1 and a binomial function in inflorescences.

UIF1 and *ULT1* have overlapping functions during flower morphogenesis

To assess whether *UIF1* functions in the same developmental processes as *ULT1*, we analysed two independent *A. thaliana* T-DNA insertion lines (Fig. 3A). The *uif1-1* allele contains a T-DNA insertion 132 bp upstream of the stop codon, creating an early stop codon 72 bp after the insertion (Fig. 3A). In the *uif1-3* allele, the T-DNA is located in the promoter region, 255 bp upstream of the start codon (Fig. 3A). RT-PCR analyses on inflorescences showed that for both homozygous mutants, no cDNA could be detected for the full-length *UIF1* transcript (Fig. 3B). In the *uif1-1* line, the transcript detected upstream of the T-DNA insertion site would result in the synthesis of a truncated UIF1 protein lacking the predicted NLS domain and the C-terminus EAR-like motif (Fig. 3A). Whether the truncated transcript detected in *uif1-1* translates into the production of a truncated protein or no protein at all remains to be addressed. We found that both *uif1* mutant alleles produce flowers with more sepals and more petals than the WT control (Fig. 3C,D,G,H,K,L,O,P; Table 1), a phenotype reminiscent of that observed in *ult1* mutants (Fletcher, 2001; Carles et al., 2005). In addition, flowers of both *uif1* mutants display loss of organ boundary and identity (Table 2), producing fused sepals (Fig. 3G) as well as petaloid stamens (Fig. 3I,M,Q; Fig. S4A,B) and branching stamens fused along the filament (Fig. 3I,J,N; Fig. S4C). Altogether, these observations suggest that *UIF1* regulates floral morphogenesis and controls organ number similarly to *ULT1*. Moreover, UIF1 regulates additional features in the flower, such as cell fate and organ identity.

Development (2016) 143, 1108-1119 doi:10.1242/dev.127365

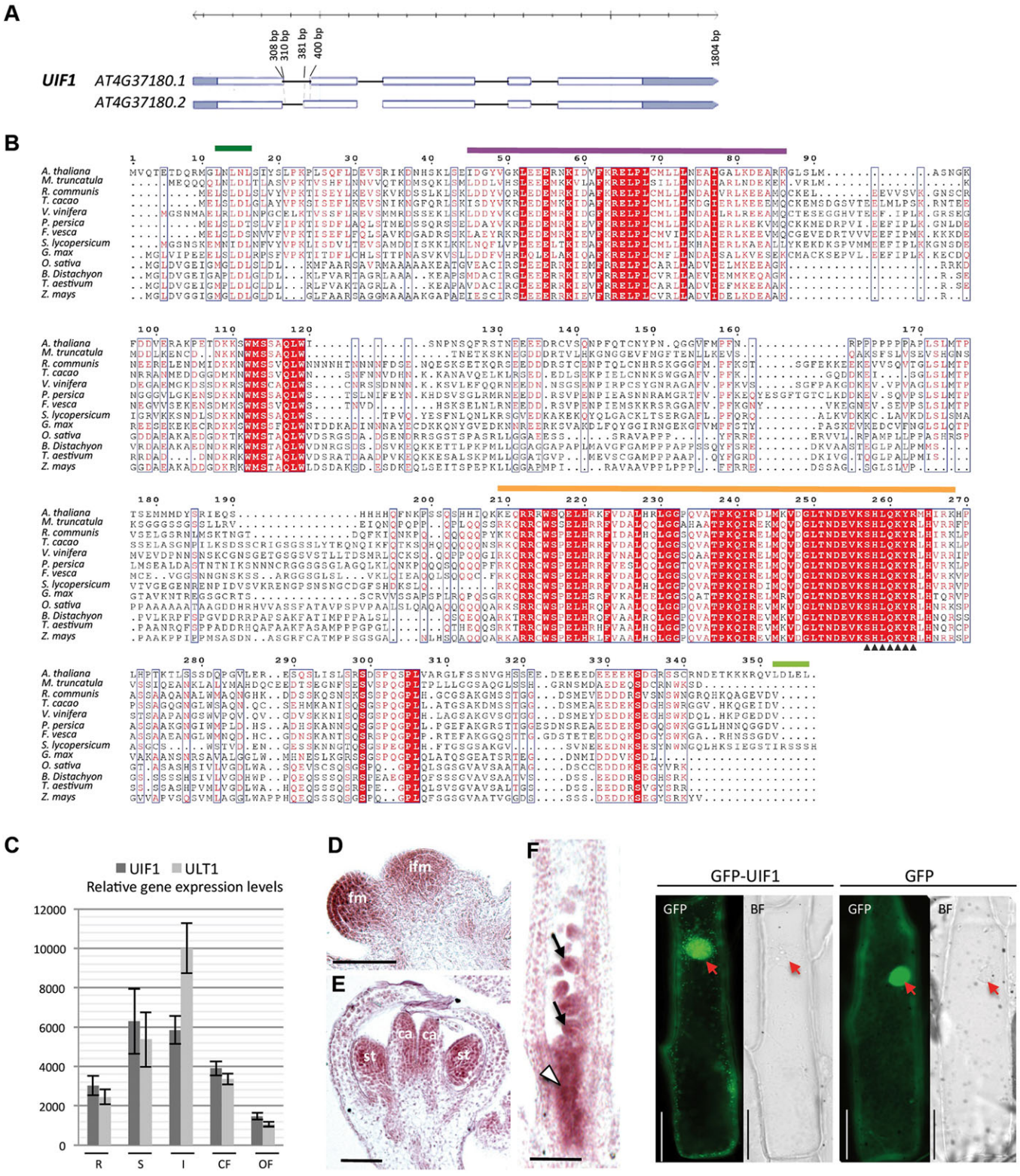

Fig. 2. See next page for legend.

ULT1 and *UIF1* function in the same pathway to control flower organ number

Whereas *ult1* mutant flowers display supernumerary organs of each type (Fletcher, 2001; Carles et al., 2005), *uif1* mutants consistently produce supernumerary sepals and petals but to a lesser extent than *ult1* mutants (Fig. 4; Table 3). To test whether *ULT1* and *UIF1* are involved in a same regulatory pathway to control organ number, *uif1-3* was crossed to the *ult1-3* null mutant. There was no significant difference between *uif1 ult1* and *ult1* mutant phenotypes for additional sepals and petals (Fig. 4; Table 3), supporting the hypothesis that *UIF1* and *ULT1* function in the same pathway for regulating organ numbers in the perianth. However, modified

Development (2016) 143, 1108-1119 doi:10.1242/dev.127365

Fig. 2. Molecular characterization of the *UIF1* gene. (A) *UIF1* gene structure and splicing variants. Blue boxes, untranslated regions (5′-, 3′-UTR); open boxes, coding regions; black lines, introns. *AT4G37180.1* (most abundant splicing variant in TAIR databases and amplified from cDNA libraries) has a first intron 21 bp longer than *AT4G37180.2*, resulting in the production of a 7-aa shorter protein (aa 75-81). (B) Alignment of predicted amino acid sequences of UIF1 (AT4G37180.1) and 12 selected orthologous proteins in dicots and monocots [*Medicago truncatula* XP_003611799.1 (68%/88% similarity with UIF1 hydrophobic domain/Myb domain, respectively), *Ricinus communis* XP_002522328.1 (83%/95%), *Theobroma cacao* XP_007047162.1 (75%/93%), *Vitis vinifera* XP_002264629.2 (80%/91%), *Prunus persica* XP_007204391.1 (80%/93%), *Fragaria vesca* XP_004288067.1 (76%/93%), *Solanum lycopersicum* XP_004233639.1 (71%/96%), *Glycine max* XP_003528384.1 (73%/83%), *Oryza sativa* Os03*g*0764600 (72%/90%), *Brachypodium distachyon* XP_003558989.1 (75%/91%), *Triticum aestivum* AEV91172.1 (72%/91%) and *Zea mays* NP_001146647.1 (76%/90%)]. Conserved amino acids are shaded in red, similar amino acids boxed in blue (>50% identity) and non-conserved amino acids in black. Dark green line, conserved EAR-like motif at the N-terminus; light green line, non-conserved EAR-like motif at the C-terminus; purple line, hydrophobic domain; orange line, Myb domain, with the SHLQKYR motif marked with triangles. (C) RT-qPCR analysis of *UIF1* (dark grey bars) and *ULT1* (light grey bars) gene expression in *A. thaliana* tissues (L*er*): roots (R), 6-day-old seedlings (S), inflorescence apices (I), closed flowers (CF) and opened flowers (OF). Values were normalised against the *EF1α* gene. Error bars indicate s.d. for three biological replicates. (D-F) Analysis of *UIF1* expression pattern in *A. thaliana* reproductive tissues (L*er*), by RNA *in situ* hybridisation (*UIF1* antisense probe). Longitudinal sections through an inflorescence meristem (ifm) with adjacent floral meristems (fm) (D), a stage 7-8 flower (st, stamen primordia; ca, carpel primordia) (E) and the pistil of a maturing flower, showing *UIF1* transcripts at the base of the gynoecium (arrowhead) and in the ovules (black arrows) (F). (G) Subcellular localisation of the GFP-UIF1 fusion protein in onion epidermis cells. GFP-UIF1 is detected in the nucleus (red arrows) and cytosolic foci. GFP control is homogeneously spread in the cytosol and nucleus. BF, bright field. Scale bars: 50 µm.

organs, such as branched stamens, were observed in flowers of *uif1 ult1* and *uif1* mutants but never in *ult1-3*, supporting an additional role of *UIF1*, independent of ULT1 function, in the control of flower organ identity.

UIF1 possesses DNA-binding sites in *WUS* promoter regions

To check whether the Myb-containing UIF1 protein is able to bind DNA on specific target sequences, a protein binding microarray (PBM) experiment (Berger and Bulyk, 2009; Godoy et al., 2011; Franco-Zorrilla et al., 2014) was performed. Analysis of DNA fragments bound by MBP-UIF1 recombinant protein yielded a series of motifs recognised with high affinity (E-score >0.45), resembling DNA sequences recognised by other transcription factors belonging to the same GARP G2-like subfamily (Franco-Zorrilla et al., 2014; Weirauch et al., 2014) (Fig. 5A). Position weight matrices of the three top-scoring motifs were used to scan regulatory sequences in putative target genes of UIF1 using Morpheus (http://biodev.cea.fr/morpheus), an algorithm that predicts binding sites in given sequences by computing affinity scores related to the used matrix (Fig. 5A). Because *uif1* mutants phenocopy *ult1* mutants, we assessed whether *WUS* could be a direct target of UIF1 (Carles et al., 2005). Hence, binding sites for UIF1 were searched and found in the promoter of *WUS*. The top two sites (Fig. S5; Fig. 5A) lie in specific regulatory regions as reported in the *WUS* promoter scanning study of Bäurle and Laux (2005). The *WUS-1* site (position −1182) is located in proximity to the quantitative element required for enhanced expression levels in the meristem, and the *WUS-2* site (position −2819) is embedded in the region for expression intensity in FM and ovule. Protein-DNA interactions were tested by an electrophoretic mobility shift assay (EMSA) using purified recombinant His-tagged GST-UIF1 fusion protein (Fig. 5A,B; Fig. S6). We found that UIF1 specifically binds the GTAGATTCCT motif (*WUS-1*), as interaction is lost upon mutation of either of two single bases at positions 5 or 8 in the sequence. Similar results were obtained when using the full-length protein or the isolated Myb domain of UIF1 fused to GST (Fig. 5B; Fig. S6). This suggests that UIF1 might directly regulate *WUS*.

UIF1 binds to DNA elements present in the *AG* gene and in CUC gene promoters

We showed in this study that UIF1 physically interacts with ULT1, previously reported to control *AG* expression. Moreover, we found that some of the *uif1* phenotypes, such as organ fusions, are reminiscent of those observed in the *cup-shaped cotyledon* (*cuc*) mutant backgrounds (Aida et al., 1997). This prompted us to seek putative UIF1-binding sites at the *AG* and CUC loci (Takada et al., 2001; Aida et al., 1997; Vroemen et al., 2003). Three UIF1 binding sites were found in *AG* regulatory sequences (Fig. 5A). Among these, the best-scored AAGAATCTTT site, present in the large regulatory intron of *AG*, was confirmed by EMSA (Fig. 5B; Fig. S6). We found that UIF1 specifically binds this motif, as interaction is lost upon mutation of a single base (c7a) in the sequence. UIF1-binding sites were also found in the promoters of the CUC genes: two in *CUC1*, three in *CUC2* and two in *CUC3* (Fig. 5A). Specific binding to motifs in the CUC genes was confirmed by EMSA (Fig. S6) and interaction with the UIF1 Myb domain was strongly reduced upon a single base mutation (a5t). These data indicate that UIF1 probably has a direct effect on *AG* and CUC gene regulation.

UIF1 has a transcriptional repressor activity

To test whether UIF1 has a role in regulating transcription, we performed a dual luciferase reporter assay (DLRA) in onion epidermis cells (Fig. 5C). For this experiment, UIF1 protein was fused to the Gal4 DNA-binding domain (G4DBD-UIF1), which binds to the upstream activation sequence (UAS) site located upstream of the CaMV*35S* minimal promoter driving the expression of firefly luciferase. The DLRA test showed that firefly luciferase expression was repressed by a mean of 2.7-fold in the presence of UIF1 (G4DBD-UIF1) compared with the inert control (G4DBD-GFP), indicating that UIF1 might function as a transcriptional repressor. Even though repression was not as efficient as for the EAR-containing protein IAA12/BODENLOS (BDL; 10.8-fold repression reduction; Szemenyei et al., 2008), we tested whether UIF1 activity was due to EAR motifs mapped at the N-terminus (EAR^N) and C-terminus (EAR^C) of the protein (Fig. 2B). We used two modified versions of UIF1: a truncated version lacking EAR^C (UIF1-dCT) or the truncated version with additional mutations in EAR^N by substituting leucines with alanines (UIF1-ANANA-dCT). Although deletion of EAR^C did not significantly affect UIF1 activity, additional mutation in EAR^N completely abolished its activity (Fig. 5C). Thus, the conserved EAR^N motif of UIF1 is necessary for transcriptional repression.

Therefore, in *A. thaliana*, UIF1 could be a transcriptional repressor of *WUS* during FM development. To investigate this, we performed RT-qPCR analyses in inflorescences of the two mutant alleles, *uif1-1* and *uif1-3*. In order to exclude *WUS* RNA derived from anthers, we used dissected inflorescences, harbouring FM younger than stage 5 (Fig. S7). We systematically found a significant increase in *WUS* expression in the mutants (Fig. 5D). This potential, direct negative regulation of *WUS* by UIF1 could explain the production of supernumerary organs by *uif1* mutant flowers, in a ULT1-dependent manner (Figs 4, 5). Indeed, we previously showed that the *WUS* expression domain was laterally enlarged in *ult1* mutants, in

Development (2016) 143, 1108-1119 doi:10.1242/dev.127365

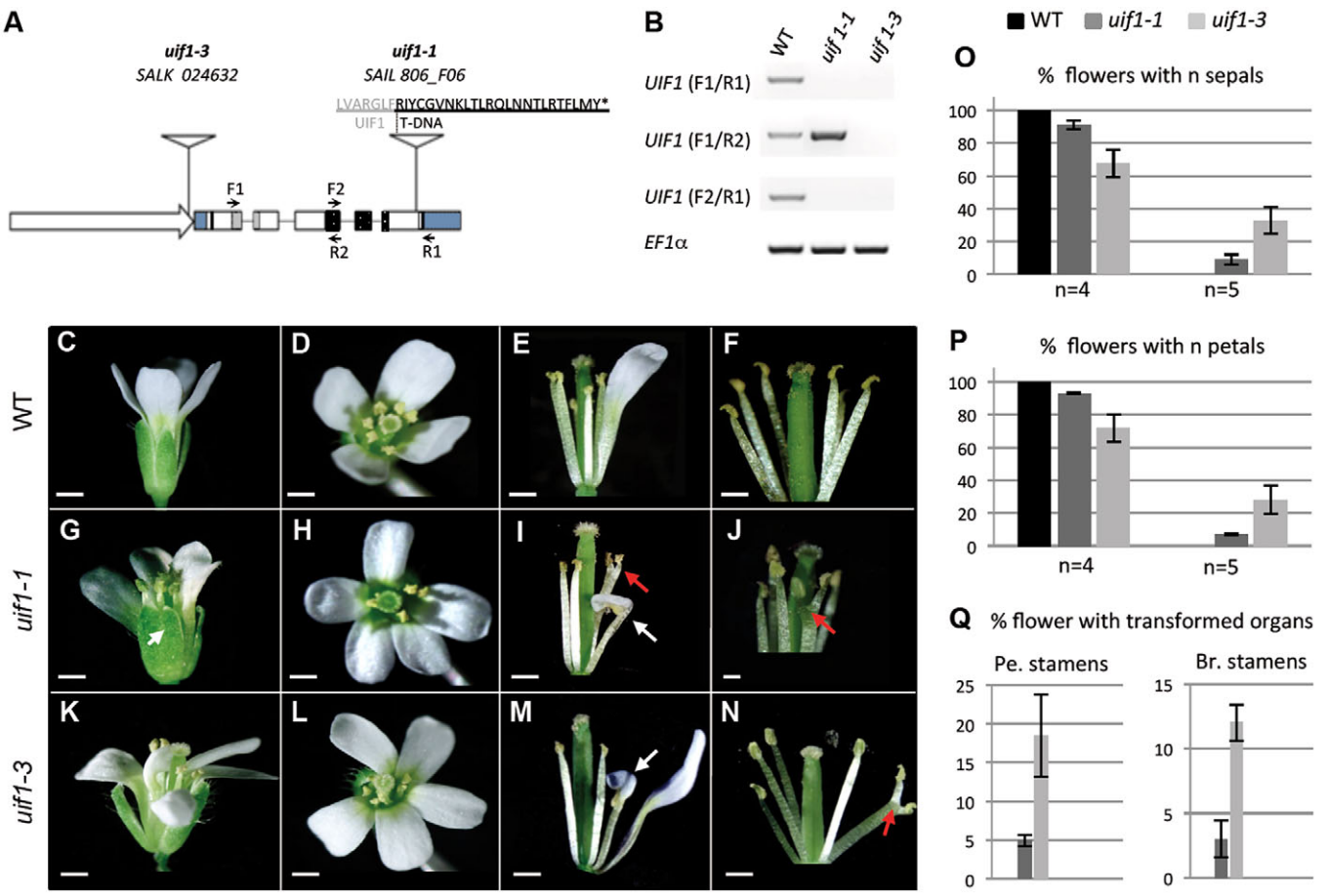

Fig. 3. *uif1-1* and *uif1-3* mutant alleles display supernumerary floral organs and loss of floral organ identity. (A) Diagram of *UIF1* genomic region and location of the T-DNA insertions in *uif1* mutant lines. Promoter (white arrow), 5′- and 3′-UTR (blue boxes), coding regions (boxes) with hydrophobic region (grey box), Myb domain (black dotted box), predicted NLS (white box) and two distinct EAR-like motifs (small black boxes close to N- and C-terminal UTR regions). The C-terminal predicted protein sequence for *uif1-1* appears on top of the diagram. Arrows indicate primers used for RT-PCR (B). (B) RT-PCR analysis of *UIF1* expression in inflorescences of mutant lines. In both *uif1-1* and *uif1-3*, cDNA corresponding to the entire *UIF1* transcript could not be detected. *EF1α*: control. (C-N) Abnormal flower development in *uif1* mutants. *uif1-1* and *uif1-3* flowers contain additional sepals (G,K) and petals (H,L), compared with WT (C,D). *uif1* flowers carry fused sepals (white arrow in G), petaloid stamens (white arrows in I,M) and branching stamens (red arrows in I,J,N,). Scale bars: 1 mm. (O-Q) Organ number and transformed organs counted in *uif1* mutant flowers. (O,P) Percentage of flowers with four or five sepals (O) and petals (P) or with transformed organs (Q; Pe, petaloid stamens; Br, branching stamens) counted from 300 flowers per line. Error bars represent s.d. for three biological replicates.

a L*er* background (Carles et al., 2005). Interestingly, and as expected in view of the relative phenotypic intensities, *uif1* mutant alleles show a weaker increase in *WUS* expression relative to the *ult1-3* null mutant in a Col-0 background (Fig. 5D).

DISCUSSION

ULT1 and UIF1 regulate homeostasis of floral meristem in a same pathway

Here, we report *in vivo* physical interaction between ULT1 and the novel Myb transcription factor UIF1 (Figs 1, 2). UIF1 was isolated from a Y2H screen against ULT1. The interaction was further confirmed in plants, where BiFC took place in the nucleus. We show that the UIF1 N-terminus region is necessary and that the ULT1 C-terminus region containing the B-box is sufficient to mediate the interaction. This is strongly supported by reports in plants showing that the B-box domain is involved in protein-protein interactions (Datta et al., 2006, 2007; Gangappa et al., 2013). In particular, the formation of heterodimers both within and outside the B-box-containing protein family play important roles in regulating transcription and fine-tuning plant growth and development (Gangappa and Botto, 2014).

Both *ULT1* and *UIF1* genes are expressed from early stages of *A. thaliana* vegetative development and have overlapping expression patterns in inflorescence and floral meristems. However, the levels of expression of *ULT1* and *UIF1* differ in floral organs or developmental stages. Interestingly, the differences seem to be associated with the developmental status of organs, *ULT1* being expressed at higher levels in dividing tissues and *UIF1* being expressed at higher levels in differentiating tissues.

Similarly to *ult1* mutants, *uif1* mutants display supernumerary floral organs (Fig. 3). In *ult1* mutants, increase of floral organ numbers correlates with inflorescence and floral meristem enlargement (Fletcher, 2001) and with lateral enlargement of the

Table 1. Supernumerary organs in *uif1* mutant alleles

	Percentage of flowers exhibiting phenotype (±s.d.)		
Phenotype	*uif1-1*	*uif1-3*	L*er* WT
More than four sepals	12±3	37±8	0
More than four petals	8±1	28±9	0

n=300 flowers per genotype.

Development (2016) 143, 1108-1119 doi:10.1242/dev.127365

Table 2. Modified organs in *uif1* mutant alleles

	Percentage of flowers exhibiting phenotype (±s.d.)		
Phenotype	*uif1-1*	*uif1-3*	Ler WT
Fused sepals	5±3	13±4	0
Petaloid stamens	5±1	18±5	0
Branching stamens	4±2	12±2	0

n=300 flowers per genotype.

Table 3. Supernumerary or modified organs in *uif1 ult1* double and single mutants*

	Percentage of flowers exhibiting phenotype (±s.d.)		
Phenotype	*uif1-3 ult1-3*	*uif1-3*	*ult1-3*
Five to eight sepals	58±2	18±3	52±2
Five to eight petals	57±4	18±3	53±3
Gynoecium with three locules	28±1	0	25±4
Branching stamens	6±1	7±1	0

n=300 flowers per genotype.
*Double and single mutants were selected from the same F2 population obtained from a cross between *uif1-3* and *ult1-3* mutants.

WUS domain of expression (Carles et al., 2005). Flowers of *ult1 uif1* double and *ult1* single mutants produce a similar number of additional sepals and petals (Fig. 4), indicating that ULT1 and UIF1 function in the same regulatory pathway for the production of perianth founder cells. The low penetrance of *uif1* phenotypes, together with their moderate intensity, do not allow measurement of meristem size differences, nor enlargement of the WUS expression domain. However, we found a slight increase in *WUS* transcript level in both *uif1* mutant alleles (Fig. 5). Together, these findings indicate that ULT1 and UIF1 might function together in OC size regulation.

UIF1 could provide DNA-binding specificity for ULT1 at target loci such as *WUS*

ULT1 was previously proposed to act through WUS to regulate meristem homeostasis (Carles et al., 2004), functioning as a negative regulator of *WUS* expression in inflorescence and floral meristems (Carles et al., 2005). Although ULT1 protein contains a SAND domain shown to act as a DNA-binding module in animals (Bottomley et al., 2001; Surdo et al., 2003) and although ULT1 protein shows general affinity for DNA, no evidence for ULT1 binding at the *WUS* locus was reported thus far, nor that ULT1 protein could recognise specific DNA motifs (Carles and Fletcher, 2009; Engelhorn et al., 2014a). In the present study, we show that UIF1 is able to bind DNA and can recognise motifs in the promoter sequence of WUS. Scanning of the entire promoter using UIF1 PBM-generated matrices led to relevant binding sites in regions previously reported as general, meristem or stem cell quantitative elements (QEs) (Fig. S5; Bäurle and Laux, 2005).

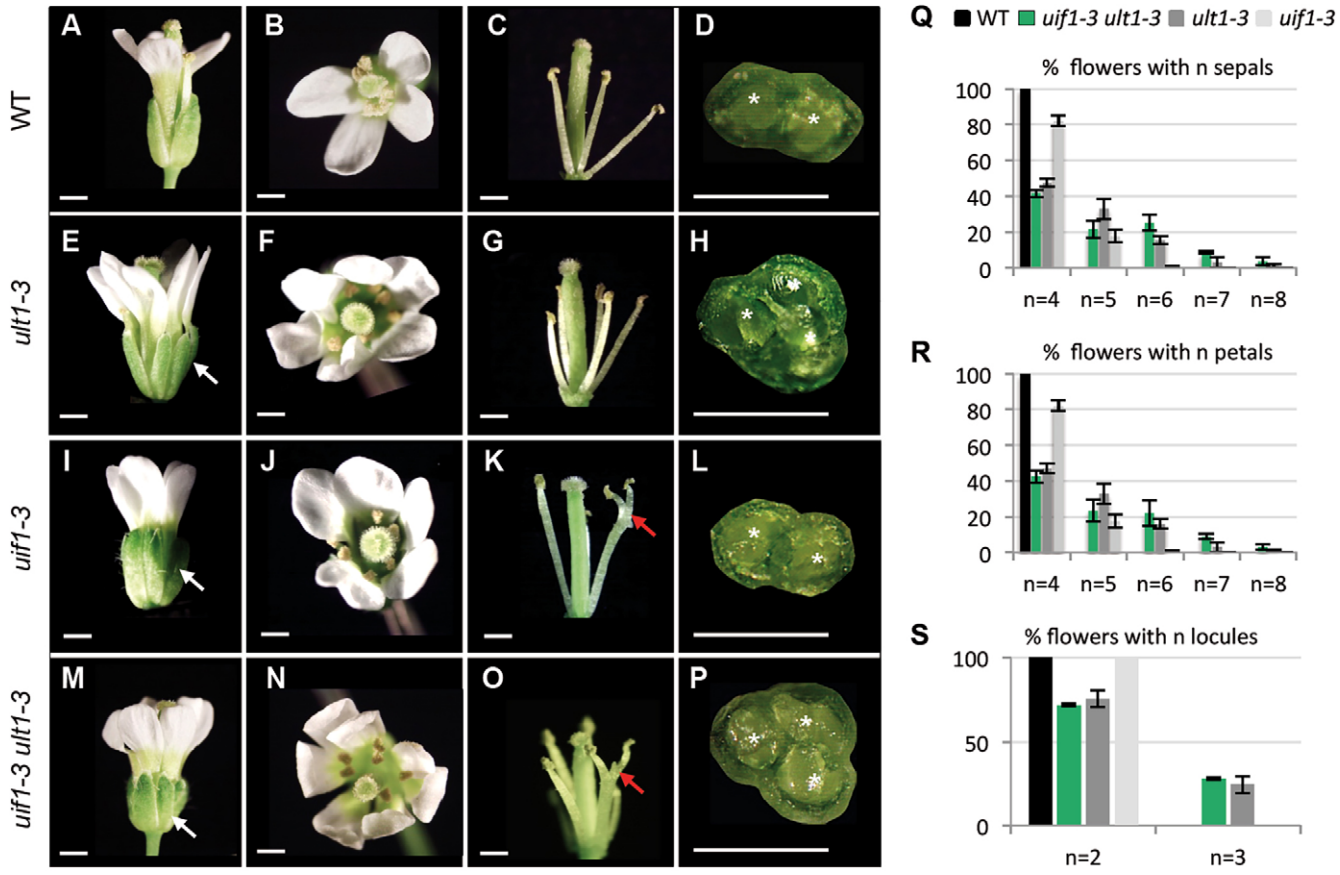

Fig. 4. *ULT1* and *UIF1* control floral organ number in the same pathway. (A-P) Phenotypes of *uif1-3 ult1-3* double and single mutants, including additional sepals (white arrows in E,I,M); pistils (P) with locules (asterisks in D,H,L,P); branching stamens (red arrows in K,O). Scale bars: 1 mm. (Q-S) Graphs showing percentage of flowers with supernumerary floral organs. (Q,R) Percentage of flowers carrying from four to eight sepals (Q) or petals (R), and two or three locules (S), counted from 300 flowers per line. Error bars represent s.d. χ^2 tests showed that each of the *uif1 ult1*, *uif1* and *ult1* populations was homogeneous (α-level=0.05) and that there was no significant difference between *uif1 ult1* and *ult1* mutants for additional floral organs (α-level=0.02 for sepal or petal number; 0.001 for locule number).

Development (2016) 143, 1108-1119 doi:10.1242/dev.127365

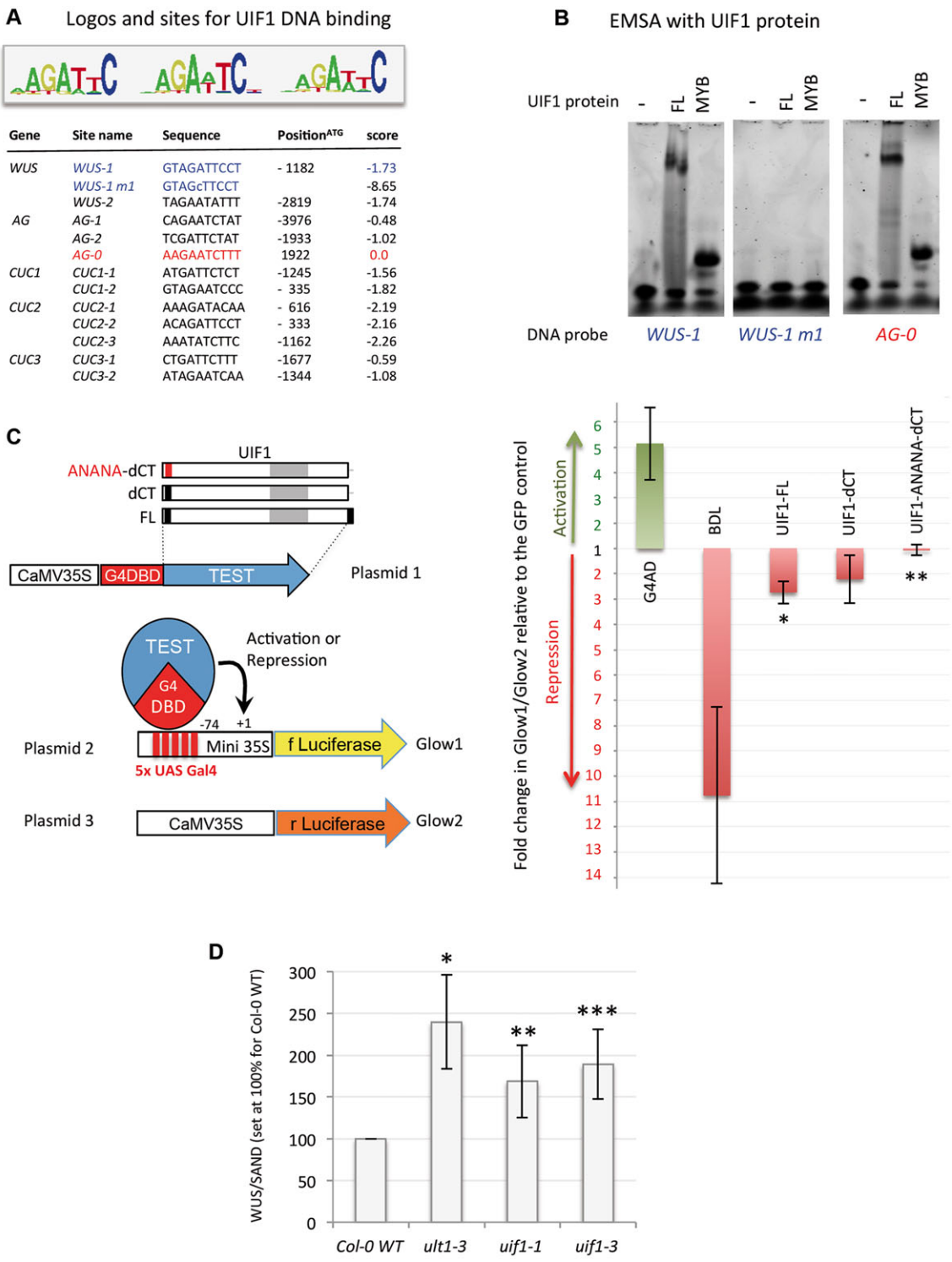

Gene	Site name	Sequence	Position^{ATG}	score
WUS	*WUS-1*	GTAGATTCCT	- 1182	-1.73
	WUS-1 m1	GTAGcTTCCT		-8.65
	WUS-2	TAGAATATTT	-2819	-1.74
AG	*AG-1*	CAGAATCTAT	-3976	-0.48
	AG-2	TCGATTCTAT	-1933	-1.02
	AG-0	AAGAATCTTT	1922	0.0
CUC1	*CUC1-1*	ATGATTCTCT	-1245	-1.56
	CUC1-2	GTAGAATCCC	- 335	-1.82
CUC2	*CUC2-1*	AAAGATACAA	- 616	-2.19
	CUC2-2	ACAGATTCCT	- 333	-2.16
	CUC2-3	AAATATCTTC	-1162	-2.26
CUC3	*CUC3-1*	CTGATTCTTT	-1677	-0.59
	CUC3-2	ATAGAATCAA	-1344	-1.08

Fig. 5. UIF1 binds to DNA motifs present in *WUS*, *AG* and *CUC* genes and has transcriptional repressor activity. (A) Logos for PBM-deduced UIF1-binding motifs, and sequences of binding sites identified in *WUS*, *CUC1-3* and *AG* genes. (B) Sequences in blue and red in A (best-scored UIF1 binding sites in *WUS* and in *AG*, or mutated version) were tested by EMSA, using the full-length UIF1 protein (6His-GST-UIF1, FL) or the Myb domain (6His-UIF1-Myb, MYB). –, sample without protein. (C) Dual luciferase reporter assay using UIF1 and controls. Left: Schematic of the constructs and the three-plasmid system. Plasmid 1: UIF1 variants fused to the Gal4 DNA-binding domain (G4DBD) specific to the Gal4 5xUAS cloned upstream of the −74 bp *CaMV35S* (mini35S) and controlling expression of the firefly luciferase gene (fLuciferase, Plasmid 2). Plasmid 3: internal transfection control using the *Renilla* luciferase gene (rLuciferase) under the control of full length *CaMV35S* promoter (CaMV35S). Right: Graph representing transcriptional activity expressed as (Glow1/Glow2) normalised to the basal activity of G4DBD-GFP set at 1. G4AD, Gal4 activating domain used as activation control; BDL, BODENLOS/IAA12 used as repression control. *P*-values calculated by *t*-test: **P*=2.59×10^{-3}, significant repressive effect of UIF1-FL compared with GFP; ***P*=0.13×10^{-3}, significant loss of repressive effect for UIF1-ANANA-dCT compared with UIF1-FL. The difference between UIF1-dCT and UIF1-FL repressive effects is not significant (*P*=0.13). (D) RT-qPCR analysis of *WUS* gene expression in dissected inflorescences (with FM younger than stage 5) of Col-0 WT, *ult1-3*, *uif1-1* and *uif1-3* mutant alleles. *WUS* expression levels were normalised against the *SAND* gene. Error bars indicate s.d. *P*-values (*t*-test) for differences with Col-0 WT: **P*=1.32×10^{-3}; ***P*=4.60×10^{-3}; ****P*=1.91×10^{-3}.

Development (2016) 143, 1108-1119 doi:10.1242/dev.127365

We showed by EMSA that UIF1 specifically binds to a site proximal to the meristem QE and that a single base mutation abolishes the binding (Fig. 5; Fig. S6). Because UIF1 protein possesses a repressor activity (Fig. 5), a reasonable hypothesis is that UIF1 binds to *WUS* and directly contributes to repress its transcription. This hypothesis is supported by the increased *WUS* expression in the inflorescences of both *uif1* mutant alleles. Moreover, UIF1 might provide DNA-binding specificity and contribute to ULT1 recruitment at the *WUS* locus for further repression via chromatin modifications. The respective mutant phenotypes support this scenario, as *ult1* defects are stronger than those of *uif1*.

Several recent studies have shown that binding of some transcriptional factors to their targets may occur prior to recruitment of the chromatin-modifying machinery, defining them as pioneers for transcriptional activation of target genes (Smale, 2010; Magnani et al., 2011; Zaret and Carroll, 2011; Iwafuchi-Doi and Zaret, 2014). In particular in plants, a pioneer function was proposed for the MADS domain-containing proteins functioning in transcriptional activation of flower morphogenesis genes (Pajoro et al., 2014). It is very likely that, via early binding to target loci, these pioneer factors could function to increase accessibility of the locus, by recruiting chromatin remodellers and modifiers (Smaczniak et al., 2012). UIF1 could be another of these TFs that recruits chromatin regulators to their targets for further regulation of chromatin accessibility. Of relevance to the important function of ULT1 in *AG* temporal activation at the centre of the FM, it cannot be excluded that UIF1 could be required to bring ULT1 to *AG* cis-regulatory elements in the proximal promoter and large intron region (Carles and Fletcher, 2009; 2010). Indeed, we found that UIF1 can specifically bind to *AG* cis-regulatory sequences located in both the promoter and the large intron, regions that we previously reported as bound by ULT1 in chromatin immunoprecipitation experiments (Carles and Fletcher, 2009).

How can we reconcile this hypothesis with a potential transcriptional repressor function, as shown by DLRA experiments? UIF1 might sit on the *AG* locus at early stages of FM development, preventing its expression, and upon an unknown signal around stage 3, bind to ULT1 protein, leading to further recruitment of chromatin factors, such as ATX1, for enrolment of the RNA PolII complex and transcriptional initiation. An alternative hypothesis is that UIF1 could carry a dual function on transcriptional regulation, depending on its interactors, acting either as repressor or as activator, as already reported for several transcription factors in *A. thaliana*, such as WUS, AP2 and FIL (Ikeda et al., 2009; Yant et al., 2010; Bonaccorso et al., 2012).

UIF1 functions in maintaining flower organ identity or spatial boundaries

The *uif1* mutants display organ fusions at their sepals and stamens. Furthermore, stamens of these mutants partially lose their identity and tend to become petaloid. Such phenotypes were observed in *uif1* and *uif1 ult1* plants but never in *ult1* mutants. This supports additional roles of *UIF1* in the control of floral organ identity and patterning that are independent of *ULT1* function. Interestingly, the organ fusion phenotypes are reminiscent of those observed in *cuc* mutants (Aida et al., 1997; Takada et al., 2001). CUC genes encode NAC domain transcription factors that specify boundaries between meristematic and primordia cells, as well as lateral organ separation (Aida et al., 1997; Takada et al., 2001; Vroemen et al., 2003; Breuil-Boyer et al., 2004; Cheng et al., 2012). Thus, mutations in these genes result in sepal fusions and stamens branching with variable strengths ranging from partial to complete fusion depending on genetic backgrounds, such as single or multiple mutants in pairwise combination (Aida et al., 1997; Takada et al., 2001; Vroemen et al., 2003). The fact that CUC promoters contain UIF1-binding sites therefore suggests that UIF1 directly influences CUC gene expression (Fig. 5; Fig. S6). However, further investigations would be required to address this hypothesis.

The fact that *AG* also contains UIF1-binding sites might explain the loss of stamen identities and the development of petaloid stamens observed in *uif1* mutants. Indeed, a decrease of *AG* expression in the developing third whorl would promote an expression of A-class genes in this domain and therefore the development of petals in place of stamens. The decrease of *AG* expression is probably very mild, thus explaining the low rate of partial homeotic transformations observed in *uif1* backgrounds. However, we cannot exclude the possibility that this phenotype also results from boundary defects between whorls 2 and 3. Such hypotheses would suggest again that UIF1 may be either an activator or a repressor of transcription, promoting here activation of *AG* expression but repressing *WUS* expression in other domains.

MATERIALS AND METHODS

Plant material and growth conditions

The *A. thaliana* Columbia-0 (Col-0) and Landsberg *erecta* (L*er*) ecotypes were used as the WT strains for the *uif1* and *ult1* alleles, respectively. Tobacco (*Nicotiana benthamiana*) plants and onion epidermis were used for transient experiments. The *uif1-1* (SAIL_806_F06) and *uif1-3* (SALK_024632) T-DNA insertional mutant lines were backcrossed two times to Col-0 before analysis. Although a third mutant allele initially named *uif1-2* (SALK-073584) putatively contains an insertion in the *UIF1* gene, we could not confirm the presence of a T-DNA at the locus in this line. Double mutant plants are in a mixed L*er* (from *ult1-3*)/Col (*uif1* alleles) background. As controls, we used single mutants in a mixed background obtained in the F2 generation from the same cross. *A. thaliana* plants were cultivated under long-day conditions (16 h light/8 h dark) at 18°C/16°C degrees. Tobacco plants were cultivated under long-day conditions (16 h light/8 h dark) at 22°C degrees. DNA material and cloning procedures are detailed in supplementary Materials and Methods.

Analysis and alignment of protein sequences

Sequences of hydrophobic and Myb conserved domains were submitted to GlobPlot (http://globplot.embl.de/cgiDict.py) for prediction of structured domains and to BlastP (http://blast.ncbi.nlm.nih.gov/) for calculation of percentages of similarity. Sequences were aligned using the MultAlin program (Corpet, 1988) and designed under ESPript3.0 (Robert and Gouet, 2014).

Yeast two-hybrid (Y2H) screen

For binary interaction tests, ULT1 and UIF1 full-length and truncated versions were expressed as Gal4 DNA-BD (BD: binding domain) or Gal4 AD (AD: activation domain) fusion proteins. *ULT1* and *UIF1*-transformed yeast strains were mated and the resulting diploids were selected for the presence of both plasmids with medium lacking Leu and Trp (−LT). The selected strains were then dotted on −LT or –LTAH medium (lacking Leu, Trp, His and Ade) on which only the diploids presenting protein interactions can grow. For more details on the Y2H screen and protein extraction for western blot on mated Y2H diploids, see supplementary Materials and Methods.

Bimolecular fluorescent complementation (BiFC) and subcellular localisation

For BiFC tests in tobacco leaf epidermis cells, constructs were transfected by agro-infiltration into leaves of 4-week-old *N. benthamiana* (Hamilton et al., 2002; Walter et al., 2004). When $OD_{600\ nm}$=0.5 was reached, *Agrobacteria* cultures were pelleted and resuspended in 10 mM $MgCl_2$ and then treated with 100 µM acetosyringone for 2 h. Tobacco leaves were infiltrated with *Agrobacteria* solutions for co-transformation allowing

Development (2016) 143, 1108-1119 doi:10.1242/dev.127365

expression of proteins fused to the N-terminal or C-terminal part of the split YFP (NY or YC). Cultures were grown separately and mixed at equal density before co-infiltration. For subcellular localisation, the pEZS-UIF1 constructs were transformed into onion epidermis cells using the Biolistic PDS-1000/He particle delivery system (Bio-Rad) (Sanford et al., 1993). The corresponding GFP-UIF fusion construct is suitable to address subcellular localisation of UIF1 protein as GFP-UIF can complement *uif1* mutants, indicating that the GFP does not affect UIF1 function. Tissues were observed 3 days after infiltration (tobacco) or 24-36 h after bombardment (onion), by epifluorescence microscopy under an Axioscope A1 (Carl Zeiss), using a 46 YFP filter (EX BP 500/20, BS FT 515, EM BP 535/30), a 49 DAPI filter (EX G 365, BS FT 395, EM BP 445/50) or a 38 Endow GFP filter (EX BP 470/40, BS FT 495, EM BP 525/50). Images were acquired using an AxioCam MRc camera equipped with the ZEN lite Module Hardware.

Dual luciferase reporter assay (DLRA)

Micro-projectiles were prepared with 50 ng of pRLC (*Renilla* luciferase construct), 400 ng of pBB168 (firefly luciferase construct; Blanvillain et al., 2011) and 15 µg of G4DBD-UIF1, G4DBD-UIF1-dCT or G4DBD-UIF1-ANANA-dCT. Onion epidermal cells were transfected as described above and kept in the dark for 20 h at 21°C, before being ground in liquid nitrogen. Proteins were extracted in 1 ml of PBLuc buffer [200 mM $NaPO_4$, pH 7, 4 mM EDTA, 2 mM dithiothreitol, 5% glycerol, 10 mg/l bovine serum albumin and EDTA-free protease inhibitor cocktail Complete (Roche)] and assayed (5-20 µl) using the Dual-Luciferase Reporter Assay System (Promega). Luciferase activities (mean±s.d.) were determined from seven independent biological replicates for each tested combination and normalised to the G4-DBD-GΔFP control set at 1.

Gene expression analyses

Total RNA extraction and RT-PCR experiments were performed as previously described (Engelhorn et al., 2014b), with 35 cycles of PCR (except for *EF1α*, 25 cycles). RT-qPCR experiments were performed in a 10 µl final volume, using 5 µl of SYBR Green Mix buffer (Bio-Rad) and 0.4 µM primers. The Bio-Rad CFX 384 real time system was used with the following program: 98°C, 2 min; 39 cycles (98°C, 5 s; 60°C, 5 s). Relative quantification (RQ) values were calculated using the $2-\Delta\Delta CT$ method (Livak and Schmittgen, 2001). ΔCt values were calculated using the *EF1α* or *SAND* genes as endogenous controls. Mean values±s.d. were calculated from three biological replicates (each quantified in three technical replicates). Sequences of *UIF1* and *WUS* primers are listed in Table S1, and those for *ULT1*, *EF1α* (At5g60390) and *SAND* (At2g28390) were already described (Carles and Fletcher, 2009; Czechowski et al., 2005).

RNA *in situ* hybridisation was performed as previously described (Carles and Fletcher, 2009). Inflorescences were harvested 4 weeks after bolting. *UIF1* sense and antisense probes were generated by T7 RNA polymerase activity from a 1-kb insert (PCR product amplified from UIF1 cDNA, using the ISH_UIF_F1/ISH_UIF_R1 primers; Table S1), cloned into the Zero Blunt PCR vector (Invitrogen).

Statistical assessment of floral organ identity and number

Counting of floral organs was carried out on the ten first flowers of first ten bolting plants for each genotype. We used the χ^2 test (Plackett, 1983) to verify that each population is homogeneous and to assess whether percentage values of additional organs counted between *uif1ult1* and *ult1* mutant lines are significantly different.

Production and purification of recombinant proteins

UIF1 protein (fused to the 6His-MBP tag for PBM experiments, or to the 6His-GST for EMSA experiments) or the UIF1 Myb domain (fused to 6His tag for EMSA experiments) were expressed in *Escherichia coli* strain Rosetta2 (DE3) (Novagen Merck Millipore), from the pETH447, pETH380 or pETH455 vector, respectively. After induction by 0.4 mM isopropyl β-D-1-thiogalactopyranoside, cells were grown overnight at 17°C. Prior to EMSA experiments, recombinant proteins were purified via their 6His tag. Pellets of 0.5 l of culture were sonicated in 50 ml lysis buffer A [500 mM NaCl, 20 mM Tris-HCl pH 8, 1 mM Tris (2-carboxyethyl)phosphine hydrochloride], containing one protease inhibitor cocktail tablet Complete EDTA-free (Roche) and centrifuged for 30 min at 13,000 ***g***. Clear supernatants were loaded on 1 ml Ni-Sepharose resin (GE Healthcare). Resin was washed with 20 volumes of buffer A containing 30 mM imidazole and eluted with buffer A containing 350 mM imidazole. The fractions containing recombinant proteins were pooled and dialysed overnight against buffer A.

Determination of UIF1 DNA-binding specificity by protein binding microarrays (PBM)

A pellet corresponding to 25 ml of an induced *E. coli* culture was stored at −80°C and resuspended in 1 ml 1× binding buffer prior to the DNA-binding assay. Synthesis of double-stranded microarray, protein incubation and immunological detection of DNA-protein complexes were performed as described (Godoy et al., 2011). We used the nPBM11 design containing 167,773 different oligonucleotide probes (Franco-Zorrilla et al., 2014) synthesised in an Agilent's SurePrint G3 4×180k format (Agilent Technologies). DNA microarray was scanned in a DNA Microarray Scanner at 2 µm resolution and quantified with Feature Extraction 9.0 software (Agilent Technologies). Normalisation of probe intensities and calculation of E-scores of all the possible 8-mers were carried out with the PBM Analysis Suite (Berger and Bulyk, 2009). Perl scripts were modified to adapt them to nPBM11 microarray dimensions and to input files generated by Feature Extraction software. Position weight matrices corresponding to top three motifs recognised with high affinity (UIF1_1ary, E-score=0.4832; UIF1_2ary, E-score=0.4814; and UIF1_3ary, E-score=0.4804) were obtained from analysis of all DNA fragments bound by the UIF1 using PBMs. These matrices were used for prediction of UIF1 binding sites in candidate targets with the Morpheus program (http://biodev.cea.fr/morpheus; Moyroud et al., 2011), using a cut-off score of −3. A score was assigned to each binding site found in candidate target genes (*WUS*, *AG*, *CUC1-3*), and only those with a score ranging from −2 to 0 (best score value) were considered for further EMSA analyses. [The best-scored AG-0 sequence is found at the 5.23×10^{-6} frequency in genome-wide regulatory regions (from a scan through the TAIR10-3 kb upstream database).] For more details of the generation of these scores, see supplementary Materials and Methods.

Electrophoretic mobility shift assays (EMSA)

For EMSA, dsDNA probes were prepared by incubating complementary single-stranded oligonucleotides (Eurofins Genomics) in annealing buffer (10 mM Tris-HCl pH 7.5, 150 mM NaCl and 1 mM EDTA). dsDNA (4 pmol) with a protruding G were fluorescently labelled with Cy5–dCTP (8 pmol) (GE Healthcare) using 1 unit of Klenow fragment polymerase (Ozyme) in 1×Klenow buffer for 1 h at 37°C. Binding reactions were performed in 20 µl binding buffer (50 mM NaCl, 10 mM Tris-HCl pH 7.5, 1% glycerol, 0.5 mM EDTA, 1 mM $MgCl_2$, 0.05 mM $ZnCl_2$ and 1% NP-40) supplemented with 28 ng/µl fish sperm DNA (Roche) and 10 nM double-stranded DNA probe. Binding reactions were loaded onto native 6% polyacrylamide gels 0.5× TBE (45 mM Tris, 45 mM boric acid and 1 mM EDTA, pH 8) and electrophoresed at 90 V for 75 min at 4°C. Gels were scanned on a Typhoon 9400 scanner [excitation light 649 nm, emission filter 670 nm band-pass filter (670 BP 30); Molecular Dynamics].

Acknowledgements

The authors thank Caroline Barette for assistance in DLRA fluorimetry dosages; Grégoire Denay and Laura Grégoire for help with binding site cut-off scores; and Aurélie Vialette-Guiraud for her help with sequence alignments and phylogenetic reconstructions. We thank Julia Engelhorn and Gilles Vachon for critical reading of the manuscript and acknowledge the Nottingham *Arabidopsis* Stock Centre (NASC) for providing insertion lines.

Competing interests

The authors declare no competing or financial interests.

Author contributions

C.C.C. and C.T. designed the project and approaches; F.M., E.T., R.B., I.L-V., J.M.F.-Z., C.T. and C.C.C. performed experiments and data analysis, with the

support of R.D., F.P. and P.M.; C.C.C. wrote the manuscript with the help of C.T. and F.M. and contribution from E.T.

Funding

This work was supported by the Rhône-Alpes county (Allocation Doctorale de Recherche, Cluster 7) [12–01293101 to F.M.]; the Centre National de la Recherche Scientifique (CNRS-Higher Education Chair, position 0428–64 to C.C.C.); the University of Grenoble-Alpes (Chaire Initiative Universitaire Alpes, UGA-UJF); and the French National Agency Young Researcher Grant [ChromFlow ANR JCJC, project SVSE2-1206 01 to C.C.C.].

Data availability

Data are available from the tair database (https://www.arabidopsis.org/servlets/TairObject?id=126622&type=locus) and the eFP Browser database (http://bbc.botany.utoronto.ca/efp/cgi-bin/efpWeb.cgi).

Supplementary information

Supplementary information available online at
http://dev.biologists.org/lookup/suppl/doi:10.1242/dev.127365/-/DC1

References

Aida, M., Ishida, T., Fukaki, H., Fujisawa, H. and Tasaka, M. (1997). Genes involved in organ separation in Arabidopsis: an analysis of the cup-shaped cotyledon mutant. *Plant Cell* **9**, 841-857.

Alvarez-Buylla, E. R., Benítez, M., Corvera-Poiré, A., Chaos Cador, A., de Folter, S., Gamboa de Buen, A., Garay-Arroyo, A., García-Ponce, B., Jaimes-Miranda, F., Pérez-Ruiz, R. V. et al. (2010). Flower development. *Arabidopsis Book* **8**, e0127.

Alvarez-Venegas, R., Pien, S., Sadder, M., Witmer, X., Grossniklaus, U. and Avramova, Z. (2003). ATX-1, an Arabidopsis homolog of trithorax, activates flower homeotic genes. *Curr. Biol.* **13**, 627-637.

Baranowskij, N., Frohberg, C., Prat, S. and Willmitzer, L. (1994). A novel DNA binding protein with homology to Myb oncoproteins containing only one repeat can function as a transcriptional activator. *EMBO J.* **13**, 5383-5392.

Bäurle, I. and Laux, T. (2005). Regulation of WUSCHEL transcription in the stem cell niche of the Arabidopsis shoot meristem. *Plant Cell* **17**, 2271-2280.

Berger, M. F. and Bulyk, M. L. (2009). Universal protein-binding microarrays for the comprehensive characterization of the DNA-binding specificities of transcription factors. *Nat. Protoc.* **4**, 393-411.

Blanvillain, R., Wei, S., Wei, P., Kim, J. H. and Ow, D. W. (2011). Stress tolerance to stress escape in plants: role of the OXS2 zinc-finger transcription factor family. *EMBO J.* **30**, 3812-3822.

Bonaccorso, O., Lee, J. E., Puah, L., Scutt, C. P. and Golz, J. F. (2012). FILAMENTOUS FLOWER controls lateral organ development by acting as both an activator and a repressor. *BMC Plant Biol.* **12**, 176.

Bottomley, M. J., Collard, M. W., Huggenvik, J. I., Liu, Z., Gibson, T. J. and Sattler, M. (2001). The SAND domain structure defines a novel DNA-binding fold in transcriptional regulation. *Nat. Struct. Biol.* **8**, 626-633.

Brand, U., Fletcher, J. C., Hobe, M., Meyerowitz, E. M. and Simon, R. (2000). Dependence of stem cell fate in Arabidopsis on a feedback loop regulated by CLV3 activity. *Science* **289**, 617-619.

Breuil-Boyer, S., Morel, P., de Almeida-Engler, J., Coustham, V., Negrutiu, I. and Tréhin, C. (2004). High-resolution boundary analysis during *Arabidopsis thaliana* flower development. *Plant J.* **38**, 182-192.

Busch, W., Miotk, A., Ariel, F. D., Zhao, Z., Forner, J., Daum, G., Suzaki, T., Christoph Schuster, C., Schultheiss, S. J., Leibfried, A. et al. (2010). Transcriptional control of a plant stem cell niche. *Dev. Cell* **18**, 841-853.

Carles, C. and Fletcher, J. C. (2003). Shoot apical meristem maintenance: the art of a dynamic balance. *Trends Plant Sci.* **8**, 394-401.

Carles, C. C. and Fletcher, J. C. (2009). The SAND domain protein ULTRAPETALA1 acts as a trithorax group factor to regulate cell fate in plants. *Genes Dev.* **23**, 2723-2728.

Carles, C. C. and Fletcher, J. C. (2010). Missing links between histones and RNA Pol II arising from SAND? *Epigenetics* **5**, 381-385.

Carles, C. C., Lertpiriyapong, K., Reville, K. and Fletcher, J. C. (2004). The ULTRAPETALA1 gene functions early in Arabidopsis development to restrict shoot apical meristem activity and acts through WUSCHEL to regulate floral meristem determinacy. *Genetics* **167**, 1893-1903.

Carles, C. C., Choffnes-Inada, D., Reville, K., Lertpiriyapong, K. and Fletcher, J. C. (2005). ULTRAPETALA1 encodes a SAND domain putative transcriptional regulator that controls shoot and floral meristem activity in Arabidopsis. *Development* **132**, 897-911.

Cheng, X., Peng, J., Ma, J., Tang, Y., Chen, R., Mysore, K. S. and Wen, J. (2012). NO APICAL MERISTEM (MtNAM) regulates floral organ identity and lateral organ separation in Medicago truncatula. *New Phytol.* **195**, 71-84.

Clark, S. E., Running, M. P. and Meyerowitz, E. M. (1993). CLAVATA1, a regulator of meristem and flower development in Arabidopsis. *Development* **119**, 397-418.

Corpet, F. (1988). Multiple sequence alignment with hierarchical clustering. *Nucl. Acids Res.* **16**, 10881-10890.

Czechowski, T., Stitt, M., Altmann, T., Udvardi, M. K. and Scheible, W. R. (2005). Genome-wide identification and testing of superior reference genes for transcript normalization in Arabidopsis. *Plant Physiol.* **139**, 5-17.

Datta, S., Hettiarachchi, G. H. C. M., Deng, X.-W. and Holm, M. (2006). Arabidopsis CONSTANS-LIKE3 is a positive regulator of red light signaling and root growth. *Plant Cell* **18**, 70-84.

Datta, S., Hettiarachchi, C., Johansson, H. and Holm, M. (2007). SALT TOLERANCE HOMOLOG2, a B-box protein in Arabidopsis that activates transcription and positively regulates light-mediated development. *Plant Cell* **19**, 3242-3255.

Ding, Y., Avramova, Z. and Fromm, M. (2011). Two distinct roles of ARABIDOPSIS HOMOLOG OF TRITHORAX1 (ATX1) at promoters and within transcribed regions of ATX1-regulated genes. *Plant Cell* **23**, 350-363.

Engelhorn, J., Blanvillain, R. and Carles, C. C. (2014a). Gene activation and cell fate control in plants: a chromatin perspective. *Cell. Mol. Life Sci.* **71**, 3119-3137.

Engelhorn, J., Moreau, F., Fletcher, J. C. and Carles, C. C. (2014b). ULTRAPETALA1 and LEAFY pathways function independently in specifying identity and determinacy at the Arabidopsis floral meristem. *Ann. Bot.* **114**, 1497-1505.

Fletcher, J. C. (2001). The ULTRAPETALA gene controls shoot and floral meristem size in Arabidopsis. *Development* **128**, 1323-1333.

Fletcher, J. C., Brand, U., Running, M. P., Simon, R. and Meyerowitz, E. M. (1999). Signaling of cell fate decisions by CLAVATA3 in Arabidopsis shoot meristems. *Science* **283**, 1911-1914.

Franco-Zorrilla, J. M., López-Vidriero, I., Carrasco, J. L., Godoy, M., Vera, P. and Solano, R. (2014). DNA-binding specificities of plant transcription factors and their potential to define target genes. *Proc. Natl. Acad. Sci. USA* **111**, 2367-2372.

Gaillochet, C., Daum, G. and Lohmann, J. U. (2015). O Cell, Where Art Thou? The mechanisms of shoot meristem patterning. *Curr. Opin. Plant Biol.* **23**, 91-97.

Gallois, J.-L., Nora, F. R., Mizukami, Y. and Sablowski, R. (2004). WUSCHEL induces shoot stem cell activity and developmental plasticity in the root meristem. *Genes Dev.* **18**, 375-380.

Gangappa, S. N. and Botto, J. F. (2014). The BBX family of plant transcription factors. *Trends Plant Sci.* **19**, 460-470.

Gangappa, S. N., Crocco, C. D., Johansson, H., Datta, S., Hettiarachchi, C., Holm, M. and Botto, J. F. (2013). The Arabidopsis B-BOX protein BBX25 interacts with HY5, negatively regulating BBX22 expression to suppress seedling photomorphogenesis. *Plant Cell* **25**, 1243-1257.

Godoy, M., Franco-Zorrilla, J. M., Pérez-Pérez, J., Oliveros, J. C., Lorenzo, O. and Solano, R. (2011). Improved protein-binding microarrays for the identification of DNA-binding specificities of transcription factors. *Plant J.* **66**, 700-711.

Gómez, E., Royo, J., Guo, Y., Thompson, R. and Hueros, G. (2002). Establishment of cereal endosperm expression domains: identification and properties of a maize transfer cell-specific transcription factor, ZmMRP-1. *Plant Cell* **14**, 599-610.

Ha, C. M., Jun, J. H. and Fletcher, J. C. (2010). Shoot apical meristem form and function. *Curr. Top. Dev. Biol.* **91**, 103-140.

Hamilton, A., Voinnet, O., Chappell, L. and Baulcombe, D. (2002). Two classes of short interfering RNA and RNA silencing. *EMBO J.* **21**, 4671-4679.

Hiratsu, K., Ohta, M., Matsui, K. and Ohme-Takagi, M. (2002). The SUPERMAN protein is an active repressor whose carboxy-terminal repression domain is required for the development of normal flowers. *FEBS Lett.* **514**, 351-354.

Holt, A. L., van Haperen, J. M. A., Groot, E. P. and Laux, T. (2014). Signaling in shoot and flower meristems of *Arabidopsis thaliana*. *Curr. Opin. Plant Biol.* **17**, 96-102.

Ikeda, M., Mitsuda, N. and Ohme-Takagi, M. (2009). Arabidopsis WUSCHEL is a bifunctional transcription factor that acts as a repressor in stem cell regulation and as an activator in floral patterning. *Plant Cell* **21**, 3493-3505.

Irish, V. F. and Sussex, I. (1992). A fate map of the Arabidopsis embryonic shoot apical meristem. *Development* **115**, 745-753.

Iwafuchi-Doi, M. and Zaret, K. S. (2014). Pioneer transcription factors in cell reprogramming. *Genes Dev.* **28**, 2679-2692.

Kinoshita, A., Betsuyaku, S., Osakabe, Y., Mizuno, S., Nagawa, S., Stahl, Y., Simon, R., Yamaguchi-Shinozaki, K., Fukuda, H. and Sawa, S. (2010). RPK2 is an essential receptor-like kinase that transmits the CLV3 signal in Arabidopsis. *Development* **137**, 3911-3920.

Laux, T. (2003). The stem cell concept in plants: a matter of debate. *Cell* **113**, 281-283.

Laux, T., Mayer, K. F., Berger, J. and Jürgens, G. (1996). The WUSCHEL gene is required for shoot and floral meristem integrity in Arabidopsis. *Development* **122**, 87-96.

Leibfried, A., To, J. P. C., Busch, W., Stehling, S., Kehle, A., Demar, M., Kieber, J. J. and Lohmann, J. U. (2005). WUSCHEL controls meristem function by direct regulation of cytokinin-inducible response regulators. *Nature* **438**, 1172-1175.

Lenhard, M. and Laux, T. (2003). Stem cell homeostasis in the Arabidopsis shoot meristem is regulated by intercellular movement of CLAVATA3 and its sequestration by CLAVATA1. *Development* **130**, 3163-3173.
Lenhard, M., Bohnert, A., Jürgens, G. and Laux, T. (2001). Termination of stem cell maintenance in Arabidopsis floral meristems by interactions between WUSCHEL and AGAMOUS. *Cell* **105**, 805-814.
Lenhard, M., Jürgens, G. and Laux, T. (2002). The WUSCHEL and SHOOTMERISTEMLESS genes fulfil complementary roles in Arabidopsis shoot meristem regulation. *Development* **129**, 3195-3206.
Leyser, H. O. and Furner, I. (1992). Characterisation of three shoot apical meristem mutants of *Arabidopsis thaliana*. *Development* **116**, 397-403.
Liu, X., Kim, Y. J., Müller, R., Yumul, R. E., Liu, C., Pan, Y., Cao, X., Goodrich, J. and Chen, X. (2011). AGAMOUS terminates floral stem cell maintenance in Arabidopsis by directly repressing WUSCHEL through recruitment of Polycomb Group proteins. *Plant Cell* **23**, 3654-3670.
Livak, K. J. and Schmittgen, T. D. (2001). Analysis of relative gene expression data using real-time quantitative PCR and the 2(-Delta Delta C(T)) Method. *Methods* **25**, 402-408.
Lohmann, J. U., Hong, R. L., Hobe, M., Busch, M. A., Parcy, F., Simon, R. and Weigel, D. (2001). A molecular link between stem cell regulation and floral patterning in Arabidopsis. *Cell* **105**, 793-803.
Magnani, L., Eeckhoute, J. and Lupien, M. (2011). Pioneer factors: directing transcriptional regulators within the chromatin environment. *Trends Genet.* **27**, 465-474.
Mayer, K. F. X., Schoof, H., Haecker, A., Lenhard, M., Jürgens, G. and Laux, T. (1998). Role of WUSCHEL in regulating stem cell fate in the Arabidopsis shoot meristem. *Cell* **95**, 805-815.
Moyroud, E., Minguet, E. G., Ott, F., Yant, L., Posé, D., Monniaux, M., Blanchet, S., Bastien, O., Thévenon, E., Weigel, D. et al. (2011). Prediction of regulatory interactions from genome sequences using a biophysical model for the Arabidopsis LEAFY transcription factor. *Plant Cell* **23**, 1293-1306.
Müller, R., Bleckmann, A. and Simon, R. (2008). The receptor kinase CORYNE of Arabidopsis transmits the stem cell-limiting signal CLAVATA3 independently of CLAVATA1. *Plant Cell* **20**, 934-946.
Ogawa, M., Shinohara, H., Sakagami, Y. and Matsubayashi, Y. (2008). Arabidopsis CLV3 peptide directly binds CLV1 ectodomain. *Science* **319**, 294.
Ohta, M., Matsui, K., Hiratsu, K., Shinshi, H. and Ohme-Takagi, M. (2001). Repression domains of class II ERF transcriptional repressors share an essential motif for active repression. *Plant Cell* **13**, 1959-1968.
Pajoro, A., Madrigal, P., Muiño, J. M., Matus, J. T., Jin, J., Mecchia, M. A., Debernardi, J. M., Palatnik, J. F., Balazadeh, S., Arif, M. et al. (2014). Dynamics of chromatin accessibility and gene regulation by MADS-domain transcription factors in flower development. *Genome Biol.* **15**, R41.
Plackett, R. L. (1983). Karl Pearson and the Chi-Squared Test. *Int. Stat.Review.* **51**, 59-72.
Prunet, N., Morel, P., Thierry, A.-M., Eshed, Y., Bowman, J. L., Negrutiu, I. and Trehin, C. (2008). REBELOTE, SQUINT, and ULTRAPETALA1 function redundantly in the temporal regulation of floral meristem termination in *Arabidopsis thaliana*. *Plant Cell* **20**, 901-919.
Prunet, N., Morel, P., Negrutiu, I. and Trehin, C. (2009). Time to stop: flower meristem termination. *Plant Physiol.* **150**, 1764-1772.
Robert, X. and Gouet, P. (2014). Deciphering key features in protein structures with the new ENDscript server. *Nucl. Acids Res.* **42**, W320-W324.
Rojo, E., Sharma, V. K., Kovaleva, V., Raikhel, N. V. and Fletcher, J. C. (2002). CLV3 is localized to the extracellular space, where it activates the Arabidopsis CLAVATA stem cell signaling pathway. *Plant Cell* **14**, 969-977.
Rose, A., Meier, I. and Wienand, U. (1999). The tomato I-box binding factor LeMYBI is a member of a novel class of myb-like proteins. *Plant J.* **20**, 641-652.
Sanford, J. C., Smith, F. D. and Russell, J. A. (1993). Optimizing the biolistic process for different biological applications. *Methods Enzymol.* **217**, 483-509.
Schaffer, R., Ramsay, N., Samach, A., Corden, S., Putterill, J., Carré, I. A. and Coupland, G. (1998). The late elongated hypocotyl mutation of Arabidopsis disrupts circadian rhythms and the photoperiodic control of flowering. *Cell* **93**, 1219-1229.
Schoof, H., Lenhard, M., Haecker, A., Mayer, K. F., Jürgens, G. and Laux, T. (2000). The stem cell population of Arabidopsis shoot meristems is maintained by a regulatory loop between the CLAVATA and WUSCHEL genes. *Cell* **100**, 635-644.
Schuster, C., Gaillochet, C., Medzihradszky, A., Busch, W., Daum, G., Krebs, M., Kehle, A. and Lohmann, J. U. (2014). A regulatory framework for shoot stem cell control integrating metabolic, transcriptional, and phytohormone signals. *Dev. Cell* **28**, 438-449.
Smaczniak, C., Immink, R. G. H., Muiño, J. M., Blanvillain, R., Busscher, M., Busscher-Lange, J., Dinh, Q. D. P., Liu, S., Westphal, A. H., Boeren, S. et al. (2012). Characterization of MADS-domain transcription factor complexes in Arabidopsis flower development. *Proc. Natl. Acad. Sci. USA* **109**, 1560-1565.
Smale, S. T. (2010). Pioneer factors in embryonic stem cells and differentiation. *Curr. Opin. Genet. Dev.* **20**, 519-526.
Sun, B., Xu, Y., Ng, K.-H. and Ito, T. (2009). A timing mechanism for stem cell maintenance and differentiation in the Arabidopsis floral meristem. *Genes Dev.* **23**, 1791-1804.
Sun, B., Looi, L.-S., Guo, S., He, Z., Gan, E.-S., Huang, J., Xu, Y., Wee, W.-Y. and Ito, T. (2014). Timing mechanism dependent on cell division is invoked by Polycomb eviction in plant stem cells. *Science* **343**, 1248559.
Surdo, P. L., Bottomley, M. J., Sattler, M. and Scheffzek, K. (2003). Crystal structure and nuclear magnetic resonance analyses of the SAND domain from glucocorticoid modulatory element binding protein-1 reveals deoxyribonucleic acid and zinc binding regions. *Mol. Endocrinol.* **17**, 1283-1295.
Szemenyei, H., Hannon, M. and Long, J. A. (2008). TOPLESS mediates auxin-dependent transcriptional repression during Arabidopsis embryogenesis. *Science* **319**, 1384-1386.
Takada, S., Hibara, K., Ishida, T. and Tasaka, M. (2001). The CUP-SHAPED COTYLEDON1 gene of Arabidopsis regulates shoot apical meristem formation. *Development* **128**, 1127-1135.
Vroemen, C. W., Mordhorst, A. P., Albrecht, C., Kwaaitaal, M. A. C. J. and de Vries, S. C. (2003). The CUP-SHAPED COTYLEDON3 gene is required for boundary and shoot meristem formation in Arabidopsis. *Plant Cell* **15**, 1563-1577.
Walter, M., Chaban, C., Schütze, K., Batistic, O., Weckermann, K., Näke, C., Blazevic, D., Grefen, C., Schumacher, C., Oecking, C. et al. (2004). Visualization of protein interactions in living plant cells using bimolecular fluorescence complementation. *Plant J.* **40**, 428-438.
Wang, G. and Fiers, M. (2010). CLE peptide signaling during plant development. *Protoplasma* **240**, 33-43.
Wang, Z. Y., Kenigsbuch, D., Sun, L., Harel, E., Ong, M. S. and Tobin, E. M. (1997). A Myb-related transcription factor is involved in the phytochrome regulation of an Arabidopsis Lhcb gene. *Plant Cell* **9**, 491-507.
Weirauch, M. T., Yang, A., Albu, M., Cote, A. G., Montenegro-Montero, A., Drewe, P., Najafabadi, H. S., Lambert, S. A., Mann, I., Cook, K. et al. (2014). Determination and inference of eukaryotic transcription factor sequence specificity. *Cell* **158**, 1431-1443.
Yadav, R. K., Perales, M., Gruel, J., Girke, T., Jönsson, H. and Reddy, G. V. (2011). WUSCHEL protein movement mediates stem cell homeostasis in the Arabidopsis shoot apex. *Genes Dev.* **25**, 2025-2030.
Yant, L., Mathieu, J., Dinh, T. T., Ott, F., Lanz, C., Wollmann, H., Chen, X. and Schmid, M. (2010). Orchestration of the floral transition and floral development in Arabidopsis by the bifunctional transcription factor APETALA2. *Plant Cell* **22**, 2156-2170.
Zaret, K. S. and Carroll, J. S. (2011). Pioneer transcription factors: establishing competence for gene expression. *Genes Dev.* **25**, 2227-2241.

SUPPLEMENTARY MATERIALS AND METHODS

Phylogenetic analyses

Sequences were aligned using the MultAlin program (Corpet, 1988) and designed under ESPript3.0 (Robert and Gouet, 2014). For phylogeny analysis, amino acid sequences from UIF1 homologues were aligned using MUSCLE in the SEAVIEW program (Gouy et al., 2010). Homologous sites for phylogenetic reconstructions were determined automatically using Gblocks. Maximum Likelihood phylogenies were then generated from these alignments in PhyML (Guindon et al., 2009) using an LG evolutionary model. The PhyML options used to generate the tree were the default settings except the invariable sites that were optimized. Statistical support was provided by aLRT (SH-like).

Mutant allele genotyping

Genotyping of *uif1-1* and *uif1-3* T-DNA insertion mutants was performed using, for gene amplification, oUIF1-ADNT06-F / oUIF1-ADNT06-R (1123 pb amplification) and oUIF1-ADNT32-F/ oUIF1-ADNT32-R (1092 pb amplification) primers, respectively; and for the presence of *uif1-1* and *uif1-3* T-DNA insertions, oUIF1-ADNT06-R RP/ oLB2 (647 pb amplification) and oUIF1-ADNT32-F/ oLBb1.3 (918 bp amplification) primers, respectively (Suppl. Table S1). The *ult1-3* allele mutant was previously described (Carles et al., 2005). Putative *uif1-3 ult1-3* double-mutant plants were identified in the F2 generation and confirmed through segregation analysis in the F3 generation.

Constructs for transient assays and transgenic plants

Bacteria expression constructs

UIF1 (At4g37180) coding sequence (cds) was amplified from an *A. thaliana* inflorescence cDNA library, using the Phusion High Fidelity DNA Polymerase (Thermo Scientific) and the oETH1239 / oETH1240 primers (Suppl. Table S1). The amplified PCR product was subcloned into Zero Blunt (Life Technologies) and further transferred into pETM-33 at NcoI-XhoI cloning sites and into pETM-41 at NcoI-NotI cloning sites. This yielded respectively the pETH380 and pETH447 expression vectors. pETM-33 allows production of recombinant proteins with a N-terminus 6His tag followed by a GST tag and by a Precission cleavage site. pETM-41 allows production of recombinant proteins with a N-terminus 6His tag followed by a MBP tag and by a tobacco etch virus (TEV) cleavage site.

The DNA fragment coding for Myb domain of UIF1 (residues 206 to 270) was amplified from pETH380 (described above) using the Phusion High Fidelity DNA Polymerase (Thermo Scientific) and oETH1415 / oETH1416 primers. The obtained PCR product was subcloned into Zero Blunt (Life Technologies) and transferred into pETM-11 at NcoI-XhoI cloning sites to yield the pETH455 expression vector. pETM-11 allows production of recombinant proteins with a N-terminus 6His tag followed by a tobacco etch virus (TEV) cleavage site.

Yeast expression constructs

ULT1 (At4g28190) cds was transferred from pEZS-ULT1-CL (Carles et al., 2005) to pGBK-T7 (Clontech) using EcoRI-BamHI restriction sites, to yield pETH198 expression vector. UIF1 was amplified from pETH380 using the Phusion High Fidelity DNA Polymerase (Thermo Scientific) and oETH1368 / oETH1369 primers, and then cloned into pGAD-T7 at the EcoRI-BamHI sites to yield the pETH390 expression vector. pGBKT7 and pGAD-T7 yeast expression vectors are designed to express proteins fused to the GAL4 DNA binding domain and the GAL4 activation domain, respectively.

The DNA fragment coding for the N-terminus part (aa 1 to 193) of ULT1 was amplified from pBB134-NY-ULT1dBbox using the Phusion High Fidelity and oETH1381 / oETH1382 primers (Suppl. Table S1). The obtained PCR product was transferred into pGBK-T7 at EcoRI-BamHI cloning sites to yield the pETH403 expression vector.

The DNA fragment coding for the C-terminus part (aa 148 to 268) of ULT1 was transferred from pEZS-CL-YC-ULT1 vectors (BiFC construct) into pGBK-T7 at EcoRI-BamHI restriction sites to yield the pETH437 yeast expression vector.

The DNA fragment coding for the SAND domain (aa 12 to 152) was amplified from pETH198 using the Phusion High Fidelity and oETH1410 / oETH1411 primers (Suppl. Table S1). The obtained PCR product was subcloned into Zero Blunt (Life Technologies) and transferred into pGBK-T7 at EcoRI-BamHI cloning sites to yield the pETH446 expression vector.

The DNA fragment coding for the C-terminus part of UIF1 (aa 91 to 356) was amplified from pETH390 using the Phusion High Fidelity and oETH1383 / oETH1384 primers (Suppl. Table S1). The obtained PCR product was transferred into pGAD-T7 at EcoRI-BamHI cloning sites to yield the pETH404 expression vector.

Plant expression constructs

For subcellular localisation, *UIF1* (At4g37180) cds was amplified from an *A. thaliana* inflorescence cDNA library, using the Phusion High Fidelity DNA Polymerase (Thermo Scientific) and the (i) oUIF1-EcoR1.F /oUIF1-BamH1nostop.R (for C-terminus fusion to GFP) or (ii) oUIF1-EcoR1.F / oUIF1-BamH1.R (for N-terminus fusion to GFP) primers (Suppl. Table S1). Each amplified PCR product was subcloned independently into Zero Blunt (Life Technologies) and further transferred into non binary vector (i) pEZS-NL-ULT1 and (ii) pEZS-CL-ULT1 (Deepgreen Stanford: hht://deepgreen.stanford.edu) at EcoRI-BamHI cloning sites (pre-digested with EcoRI-BamHI to remove ULT1 cds (At4g28190) and correspond respectively to pEZS-NL-UIF1 and pEZS-CL-UIF1 vectors.

The vectors used for BiFC for transient expression were generated from the pEZS backbone and are gift from Bassem Al Sady (UC Berkeley, PGEC, USA). They each contain cds for one of the two split YFP forms (NY: aa 1 to 166; YC aa 167 to 265) under the control of a *CaMV35S* promoter, and for fusion at the N or C-terminus end the cds of interest (four vectors in total). A terminator of the transcription site (Osc) is located at the C-terminus end of the construct. The cds of *UIF1* and *ULT1* were amplified from an *A. thaliana* inflorescence cDNA library, using the Phusion High Fidelity DNA Polymerase (Thermo Scientific) and the UIF1salI.F / oUIF1-BamH1.R, ULT1-salI.F / oULT1-BamH1.R or UIF1-SalI.F / oUIF1-BamH1nostop.R, or ULT1-SalI.F / oULT1-BamH1nostop.R primer combinations (Suppl. Table S1). Truncated versions UIF1 93-364 and ULT1 1-193 (Fig. 1A) were amplified using UIF1dNTsalI.F / oUIF1-BamH1nostop.R, or UIF1dNTsalI.F / oUIF1-BamH1.R and or ULT1-SalI.F / oULT1dBbCTBamHI.R or ULT1-SalI.F / oULT1dBbCT-nostopBamHI.R primer combinations (Suppl. Table S1). Each PCR product was subcloned independently into Zero Blunt (Life Technologies), transferred into pEZS-CL-splitYFP vectors using Sal1-BamH1 then into the binary vectors pBB130 (nptII) and pBB134 (hptII) using XhoI-XbaI. pBB130 and pBB134 are derived from pART27 vectors (Gleave, 1992) in which the GFP fusion cassette from pEZS-NL (NotI fragment; Blanvillain et al., 2011) has been inserted and/or the NPTII resistance gene has been replaced by HPTII. The 2 separate resistance genes allow selection of doubly transformed Arabidopsis plants expressing two candidate interactors in fusion to each split-YFP. The transgenes were transferred into Arabidopsis using the *Agrobacterium tumefasciens*-mediated floral dip transformation.

For DLRA assays, *UIF1* WT or mutated cds versions were amplified from an *A.thaliana* inflorescence cDNA library, using the Phusion High Fidelity DNA Polymerase (Thermo Scientific) and the oUIF_FAscI / oUIF_RXbaI , oUIF_FAscI / oUIF_RdEARXbaI or oUIF-

ANANA_FAscI / oUIF_RdEARXbaI primer couples (Suppl. Table S1). Amplified PCR products were subcloned independently into Zero Blunt (Life Technologies) and further transferred into the pBB120 binary vector at AscI-XbaI cloning sites, allowing expression of a protein fused to the Gal4 DNA-binding domain (G4DBD), namely G4DBD-UIF-FL, G4DBD-UIF-dCT or G4DBD-UIF-ANANA-dCT.

Yeast-two-hybrid (Y2H) screen

The Y2H screen was performed using the Horwitz and Ma cDNA library (CD4-30), generated from mRNAs of inflorescence meristems, floral meristems and floral buds up to stage 8 or 9. An overnight culture of the AH109 strain (Clontech) carrying the Balt vector (ULT1 fused to the Gal4 DNA Binding Domain = pETH198 described below) was performed in 5 mL of YNB medium (MP Biomedicals) containing all essential amino-acids except tryptophane. The day of transformation, this culture was diluted in 100mL to obtain a final OD (600nM) of 0.3 and was grown again until it reached an OD (600nM) of 0.8. The culture was centrifuged two times. After the first centrifugation, the pellet was resuspended in 20 mL of water and after the second centrifugation, the pellet was resuspended in 20 mL of 100 mM Lithium Acetate. After the last resuspension, the culture was centrifuged and the pellet was resuspended in 1mL of 100mM Lithium Acetate and separated in five tubes. After an incubation of one hour at 28°C with gentle shaking, in each tube, the transformation reaction was performed by adding 200 µg of denaturated carrier DNA, 5 µg of cDNA library and 1.2 mL of solution B (100 mM LiAc, 40% PEG and 1xTE). After an incubation of 30 min at 28° C with gentle shaking, a heat shock was performed in a water bath at 42°C during 15 min. After the heat shock, 700 µl of YNB medium was added to each tube to dilute the PEG. After a centrifugation, each pellet was resuspended in 1 mL of YPGA medium and incubated 1 h at 28°C. A last centrifugation was performed and each pellet was resuspended in 800 µL of YNB medium. With each tube, 2 plates of YNB with all essential amino acids excepted leucine, tryptophan, adenine and histidine were plated and incubated at 30°C. For all the colonies that grew on these plates, three successive isolations were made on YNB selectives plates, and a plasmid extraction was performed from the last yeast cultures. After extraction the plasmids were transformed into *E. coli* (HB101 strain), and grown in liquid LB medium. An extraction of plasmid was performed and the cDNA insert was sequenced.

Protein extraction and western blot on mated Y2H diploids:

A yeast culture of 5mL (OD =3) was used for the extraction of proteins from each of the Y2H diploids. Protein extraction was adapted from Volland et al. (1994). Each culture was pelleted and resuspended in 500µL of water before addition of 50µL of NaOH 1.85N and 10 minutes incubation on ice. After addition of 50µL TCA 50% and 10 minutes incubation on ice, a centrifugation was performed for 10 minutes at 13000 rpm. The pellet was washed with 500µL of Tris-HCl 1M pH8. After a centrifugation of 10 minutes at 13000rpm, the pellet was resuspended in 50µL of buffer containing 50mM Tris-HCl pH 6.8, 2mM EDTA, 2% SDS, 10% Glycerol, bromophenol blue, 2% β-Mercaptoethanol. After a denaturation step of 5 minutes at 95°C, 10µL of each sample were loaded on a gel to perform a western blot. The proteins were transfered onto a PVDF membrane (GE Healthcare) that had been previously activated in methanol for 1min. The transfer was performed during 1h at 100V in buffer containing Laemli 1x and Ethanol 20%.

For detection of the Gal4-AD fusions (western-blot with an anti-HA antibody), the membrane was blocked overnight at 4°C in a solution of TBS-T 1x (TBS and 0.1% Triton X-100) containing 10% milk. After 3 washes of 5 minutes in TBS-T, the membrane was incubated with an anti-HA antibody (Roche) at a 1:10,000 dilution. After 3 washes of 5 minutes in TBS-T, the membrane was incubated with a rat secondary antibody coupled to HRP (Sigma-Aldrich) at a 1:5,000 dilution. After 3 washes of 5 minutes in TBS-T, the detection was performed with the Clarity ECL Western Substrate kit (Biorad) using the Chemidoc MP (Biorad). For detection of the Gal4-BD fusions (western-blot with an anti-c-Myc antibody), the membrane was blocked overnight at 4°C in a PBS-T 1x (PBS and 0.6% Tween 20) solution containing 10% milk. After 3 washes of 5 minutes in PBS-T, the membrane was incubated with an anti-c-Myc antibody (clone 9e10, Covance) at a 1:5,000 dilution, in a PBS-T solution containing 10% SVL. After 3 washes of 5 minutes in PBS-T, the membrane was incubated with a mouse secondary antibody coupled to HRP at a 1:5,000 dilution. After 3 washes of 5 minutes in PBS-T, the detection was performed with the Clarity ECL Western Substrate kit (Biorad) using the Chemidoc MP (Biorad).

Cut-off score for selection of UIF1 binding sites in candidate genes from the PBM-obtained matrices

Binding matrices corresponding to the three top-scoring motifs were used for prediction of UIF1 binding sites using Morpheus. The cut-off score was defined from a scan through all *A. thaliana* 3-kb promoter sequences (TAIR10 database), using the three UIF1 matrices (UIF1_1ary, UIF1_2ary UIF1_3ary): frequencies in the genome of a 0-score are 2.38×10^{-6} [UIF1_1ary and UIF1_3ary], 1.12×10^{-5} [UIF1_2ary]; of a -1-score: 1.09×10^{-4} [UIF1_1ary], 2.85×10^{-4} [UIF1_2ary], 3.42×10^{-4} [UIF1_3ary]; of a -2-score: 5.31×10^{-4} [UIF1_1ary], 7.43×10^{-4} [UIF1_2ary], 1.36×10^{-3} [UIF1_3ary]; of a -3 score: 1.48×10^{-3} [UIF1_1ary], 1.77×10^{-3} [UIF1_2ary], 3.92×10^{-3} [UIF1_3ary]). A cut-off score of -3 allows selecting only high confidence UIF1 binding sites (p-value < 0.01). A score was assigned to each binding site found in candidate target genes (*WUS*, *AG*, *CUC1-3*), and only those with a score ranging from -2 to 0 were considered for further EMSA analyses.

SUPPLEMENTARY REFERENCES

Carles, C.C., Choffnes-Inada, D., Reville, K., Lertpiriyapong, K. and Fletcher, J.C. (2005). ULTRAPETALA1 encodes a SAND domain putative transcriptional regulator that controls shoot and floral meristem activity in Arabidopsis. *Development* **132**, 897-911.

Corpet, F. (1988). Multiple sequence alignment with hierarchical clustering. *Nucl. Acids Res.* **16,** 10881-10890.

Gouy, M., Guindon, S. and Gascuel, O. (2010). SeaView version 4: A multiplatform graphical user interface for sequence alignment and phylogenetic tree building. *Mol. Biol. Evol.* **27**, 221-224.

Guindon, S., Delsuc, F., Dufayard, J.-F. and Gascuel, O. (2009). Estimating maximum likelihood phylogenies with PhyML. *Methods Mol. Biol*. **537**, 113-137.

Robert, X. and Gouet, P. (2014). Deciphering key features in protein structures with the new ENDscript server. *Nucl. Acids Res*. **42** (Web Server Issue), W320-W324.

Volland, C., Urban-Grimal, D., Géraud, G., and Haguenauer-Tsapis, R. (1994). Endocytosis and Degradationo f the Yeast Uracil Permease Under Adverse Conditions. *J. Biol. Chem.* **269**, 9833-9841.

SUPPLEMENTARY DATA

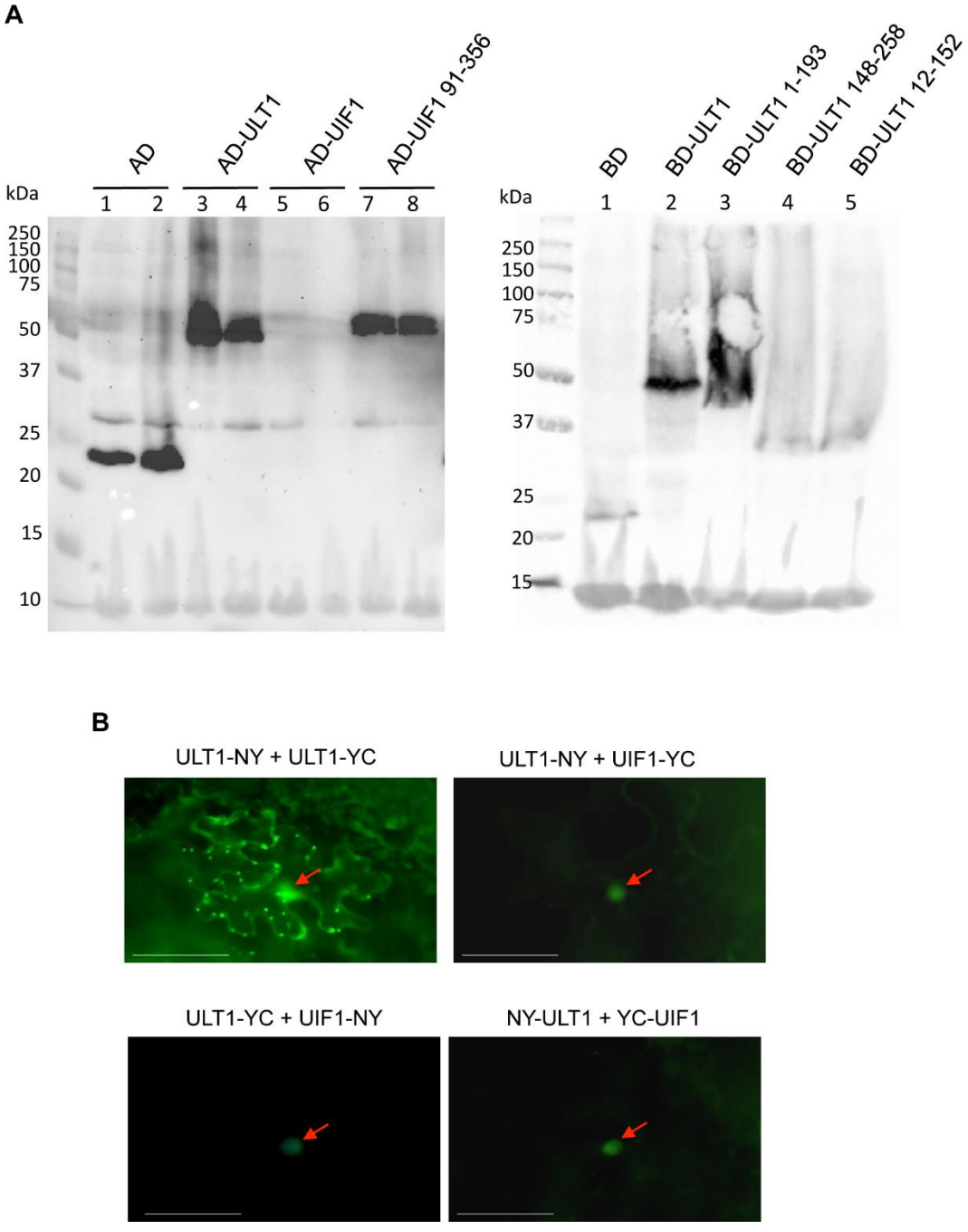

Supplementary Figure S1. Supplemental dataset for ULT1-UIF1 interaction, as tested by (A) Y2H or (B) BiFC experiments. (A) Western-blot analyses were performed on diploids obtained from mated yeast strains for co-expression of *ULT1* and *UIF1* constructs. (left) Western-blot on yeast extracts using an anti-HA antibody for detection of Gal4-AD fusions. Lane 1: mating between Gal4 DBD and Gal4 AD expression clones, lane 2: mating

between Gal4 DBD – ULT1 and Gal4 AD expression clones, lane 3: mating between Gal4 DBD and Gal4 AD – ULT1 expression clones, lane 4: mating between Gal4 DBD – ULT1 and Gal4 AD – ULT1 expression clones, lane 5: mating between Gal4 DBD and Gal4 AD – UIF1 expression clones, lane 6: mating between Gal4 DBD – ULT1 and Gal4 AD – UIF1 expression clones, lane 7: mating between Gal4 DBD and Gal4 AD - UIF1 (aa. 91 to 356) expression clones, lane 8: mating between Gal4 DBD - ULT1 and Gal4 AD - UIF1 (aa. 91 to 356) expression clones. (right) Western blot on yeast extracts using an anti-C-myc antibody, for detection of Gal4-DBD fusions. Lane 1 : mating between Gal4 DBD and Gal4 AD expression clones, lane 2 : mating between Gal4 DBD – ULT1 and Gal4 AD expression clones, lane 3 : mating between Gal4 DBD – ULT1 (aa. 1 to 193) and Gal4 AD expression clones, lane 4 : mating between Gal4 DBD – ULT1 (aa. 148 to 258) and Gal4 AD expression clones, lane 5 : mating between Gal4 DBD – ULT1 (aa. 12 to 152) and Gal4 AD expression clones. BD: DNA binding domain, AD: activation domain. (B) Supplemental dataset for ULT1-UIF1 interaction in the nucleus of tobacco cells by BiFC experiments. Cells of tobacco leaves were transiently co-infiltrated with protein fused at their C and N-ter part to N-ter part of YFP (NY) or C-ter part of YFP (YC) respectively: ULT1-NY and ULT1-YC (as control); ULT1-NY and UIF1-YC; ULT1-YC and UIF1-NY; NY-ULT1 and YC-UIF1. Tissues were observed 3 days after infiltration under Zeiss Axioplan fluorescent microscope with YFP filter (Green fluorescence) under 40 x objectives. The YFP signal detected in the nuclei of tobacco cells was reproducibly obtained in multiple independent experiments and with four different combinations of split YFP fusions to ULT1 and UIF1 proteins (Fig.1 and this Suppl. Fig. S1). Red arrows indicate cell nuclei. Scale bars: 2 µm.

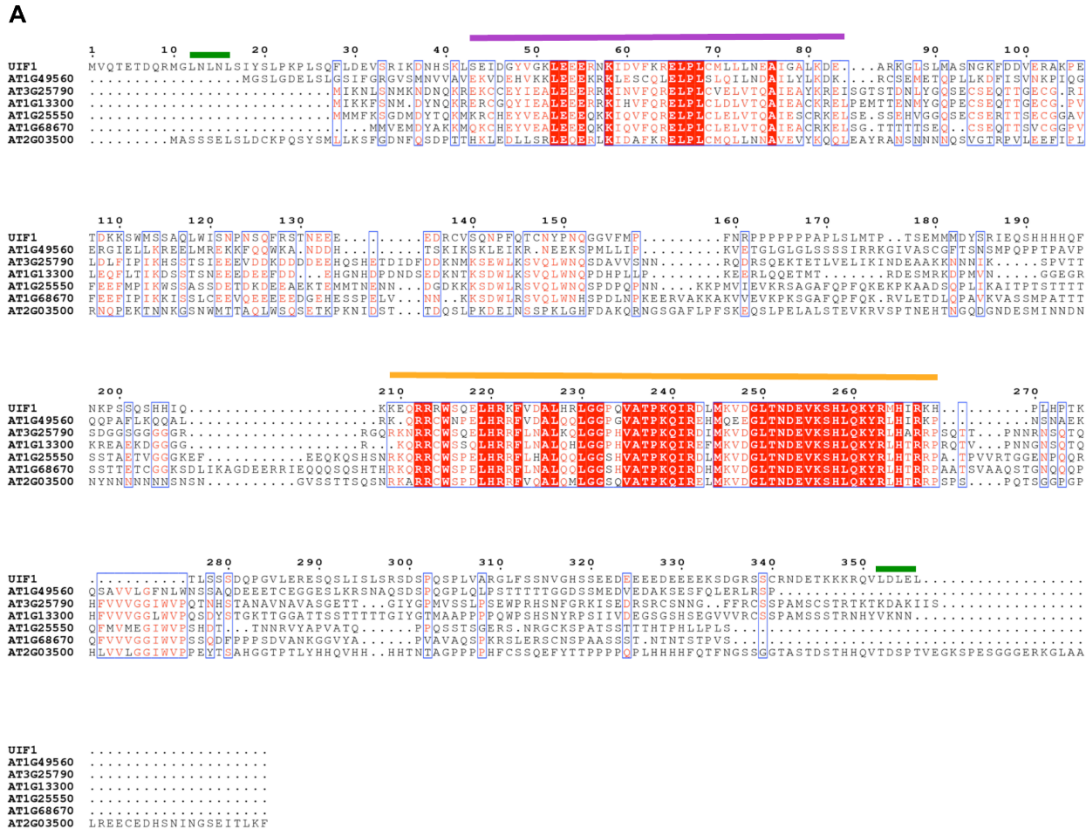

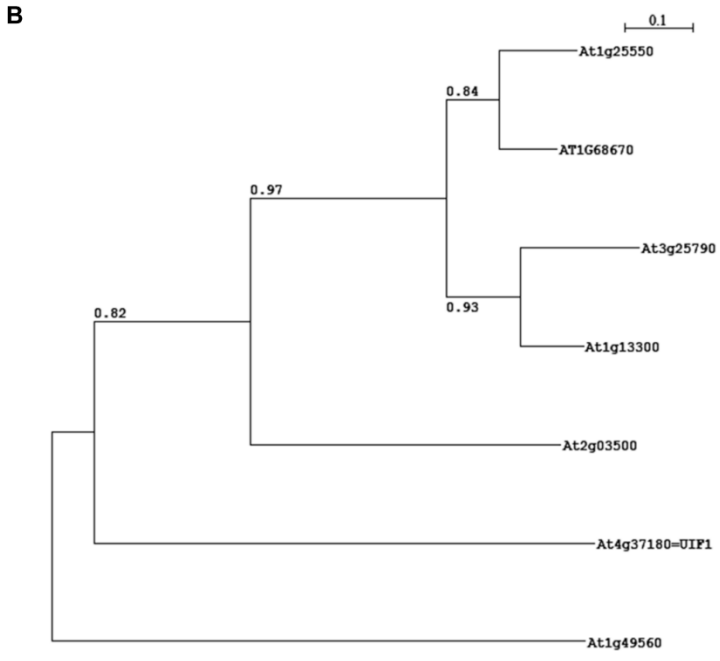

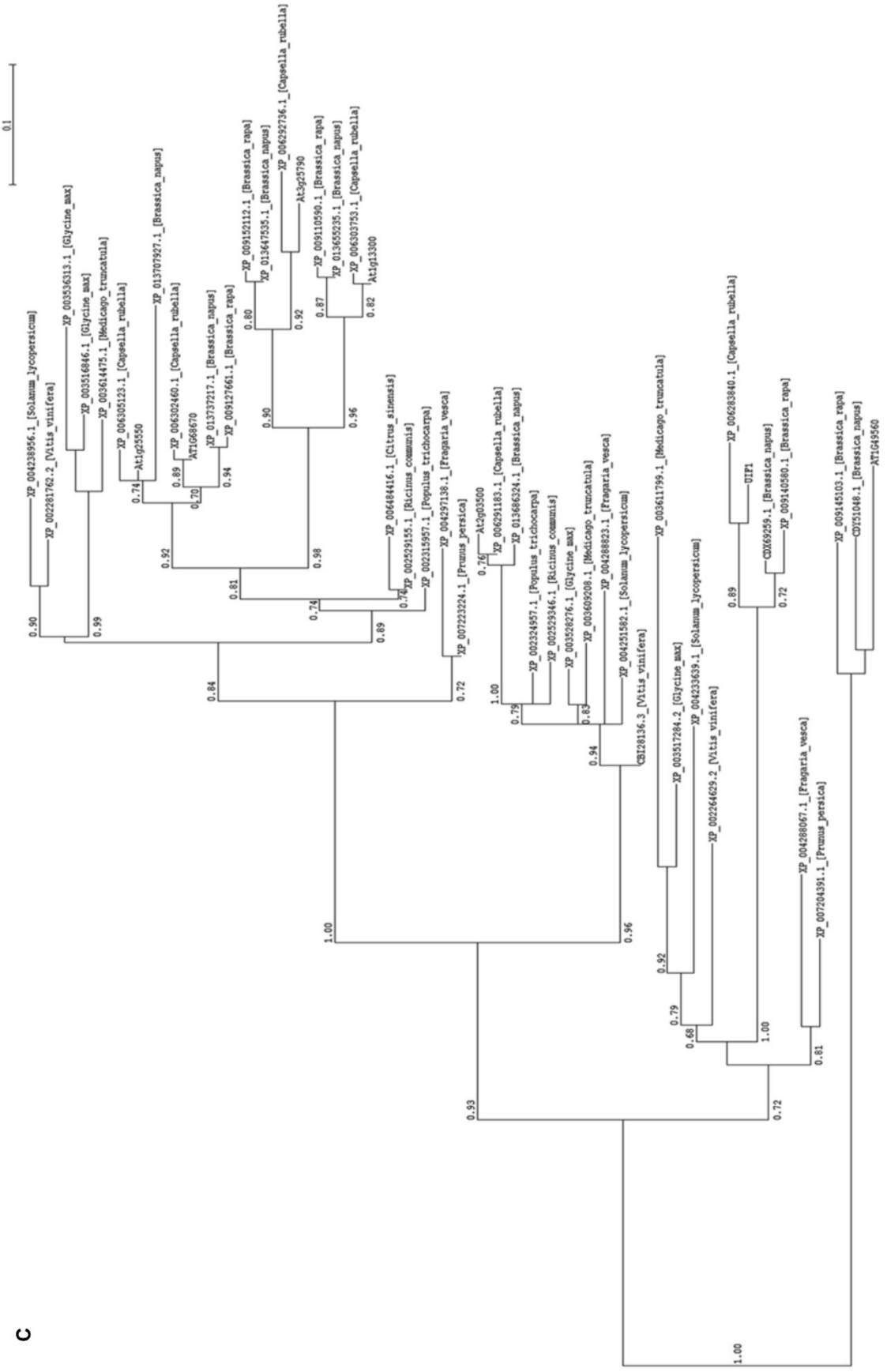
0.1
XP_004238956.1_[Solanum_lycopersicum]
XP_002281762.2_[Vitis_vinifera]
XP_003536313.1_[Glycine_max]
XP_003516846.1_[Glycine_max]
XP_003614475.1_[Medicago_truncatula]
XP_006305123.1_[Capsella_rubella]
At1g25550
XP_013707927.1_[Brassica_napus]
XP_006302460.1_[Capsella_rubella]
ATIG68670
XP_013737217.1_[Brassica_napus]
XP_009127661.1_[Brassica_rapa]
XP_009152112.1_[Brassica_rapa]
XP_013647535.1_[Brassica_napus]
XP_006292736.1_[Capsella_rubella]
At3g25790
XP_009110590.1_[Brassica_rapa]
XP_013655235.1_[Brassica_napus]
XP_006303753.1_[Capsella_rubella]
At1g13300
XP_006488416.1_[Citrus_sinensis]
XP_002529155.1_[Ricinus_communis]
XP_002315957.1_[Populus_trichocarpa]
XP_004297138.1_[Fragaria_vesca]
XP_007223224.1_[Prunus_persica]
At2g03500
XP_006291183.1_[Capsella_rubella]
XP_013686324.1_[Brassica_napus]
XP_002324957.1_[Populus_trichocarpa]
XP_002529346.1_[Ricinus_communis]
XP_003528276.1_[Glycine_max]
XP_003609208.1_[Medicago_truncatula]
XP_004288823.1_[Fragaria_vesca]
XP_004251582.1_[Solanum_lycopersicum]
CBI28136.3_[Vitis_vinifera]
XP_003611799.1_[Medicago_truncatula]
XP_003517284.2_[Glycine_max]
XP_004233639.1_[Solanum_lycopersicum]
XP_002264629.2_[Vitis_vinifera]
XP_006283840.1_[Capsella_rubella]
UIF1
CDX69259.1_[Brassica_napus]
XP_009140580.1_[Brassica_rapa]
XP_004288067.1_[Fragaria_vesca]
XP_007204391.1_[Prunus_persica]
XP_009145103.1_[Brassica_rapa]
CDY51048.1_[Brassica_napus]
ATIG49560

C

Supplementary Figure S2. Phylogenetic analyses of UIF1 and its homologues in *A. thaliana*. (A) Alignment of predicted amino acid sequences of UIF1 (AT4G37180.1) and UIF1-like homologues in *A. thaliana* (https://blast.ncbi.nlm.nih.gov/). Conserved aa are colored in red (100% identity), or boxed in blue (>50% identity) and non-conserved aa appear in black. The alignment shows that both the hydrophobic region (purple line) and the Myb domain (orange line) are conserved, while the EAR-like motifs (green lines) are specific to UIF1. (B,-C) Phylogenetic reconstructions from (A) UIF1 paralogues and (B) UIF1 orthologues in eudicots. Amino acid sequences were aligned using CLUSTALO in the SEAVIEW program (Gouy et al., 2010). Homologous sites for phylogenetic reconstructions were determined automatically using Gblocks. Maximum Likelihood phylogenies were then generated from these alignments in PhyML (Guindon et al., 2009) using an LG evolutionary model. The PhyML options used to generate the tree were the default settings except the invariable sites that were optimized. Statistical support was provided by aLRT (SH-like). Bootstraps support values superior to 0.6 are indicated at corresponding nodes.

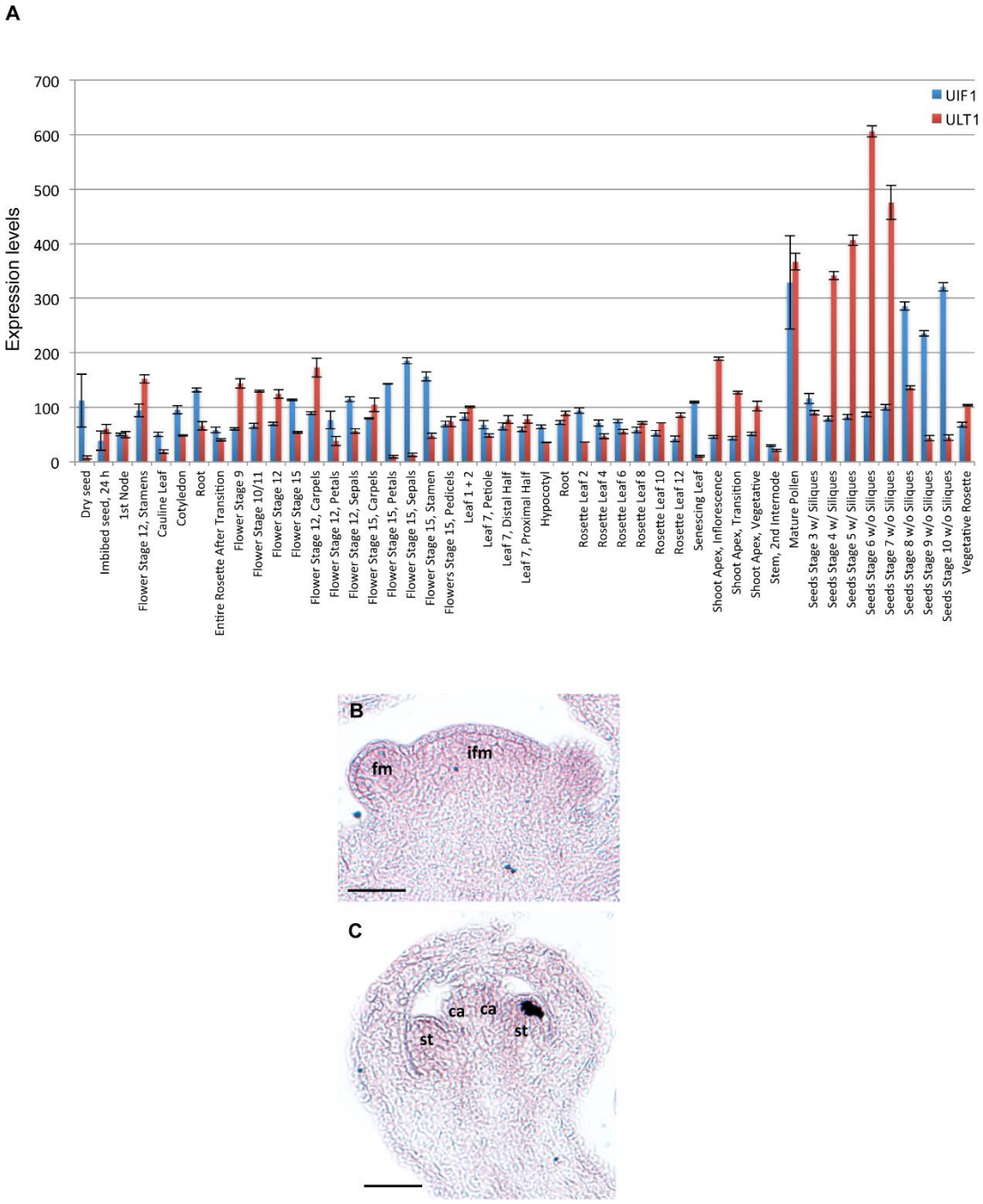

Supplementary Figure S3. UIF1 and ULT1 expression data. (A) Graphic representation of *UIF1* and *ULT1* expression levels in all tissues and organs of the *Arabidopsis thaliana* plant at different developmental stages (extracted from the eFP Browser dataset; http://bbc.botany.utoronto.ca/efp/cgi-bin/efpWeb.cgi). *ULT1* expression level (red bars) is slightly higher than the one of *UIF1* (blue bars) until stage 12 of flower development (pre-anthesis) and then, this ratio is reversed from post-anthesis stages on. Regarding relative

expressions in individual floral organs, *UIF1* expression is higher than that of *ULT1* in sepals and petals, while *ULT1* expression is higher in carpels. In seeds and siliques, *ULT1* expression is much higher than *UIF1* expression during early embryogenesis but this tendency shifts drastically during later stages of embryogenesis with *UIF1* expression being higher than *ULT1* expression. Expression levels are expressed in absolute values as in e-FP Browser, standard errors are represented by vertical bars. (B-C) RNA *in situ* hybridization control for Fig. 2 D-F, using an *UIF1* sense probe hybridized to WT L*er* tissues. Longitudinal sections (B) through the inflorescence meristem (ifm) and adjacent floral meristems (fm) or (C) through a stage 6-7 flower. st: stamen primordia; ca: carpel primordia. Scale bars: 50 µm.

Supplementary Figure S4. *uif1-1* and *3* allelic mutants display loss of floral organ identity. (A-C) Flower phenotypes of eight week-old *uif1-1* (C) and *uif1-3* (A-B) mutant plants. *uif1-1* and *uif1-3* mutant alleles produced flowers with (A-B) stamens in the third whorl (red arrows) that partially lose their identity and become petaloid (white arrow) (A, zoom in B), or (C) branching stamens (white arrow) only fused along the filament (red arrow). Scale bars: 500µm.

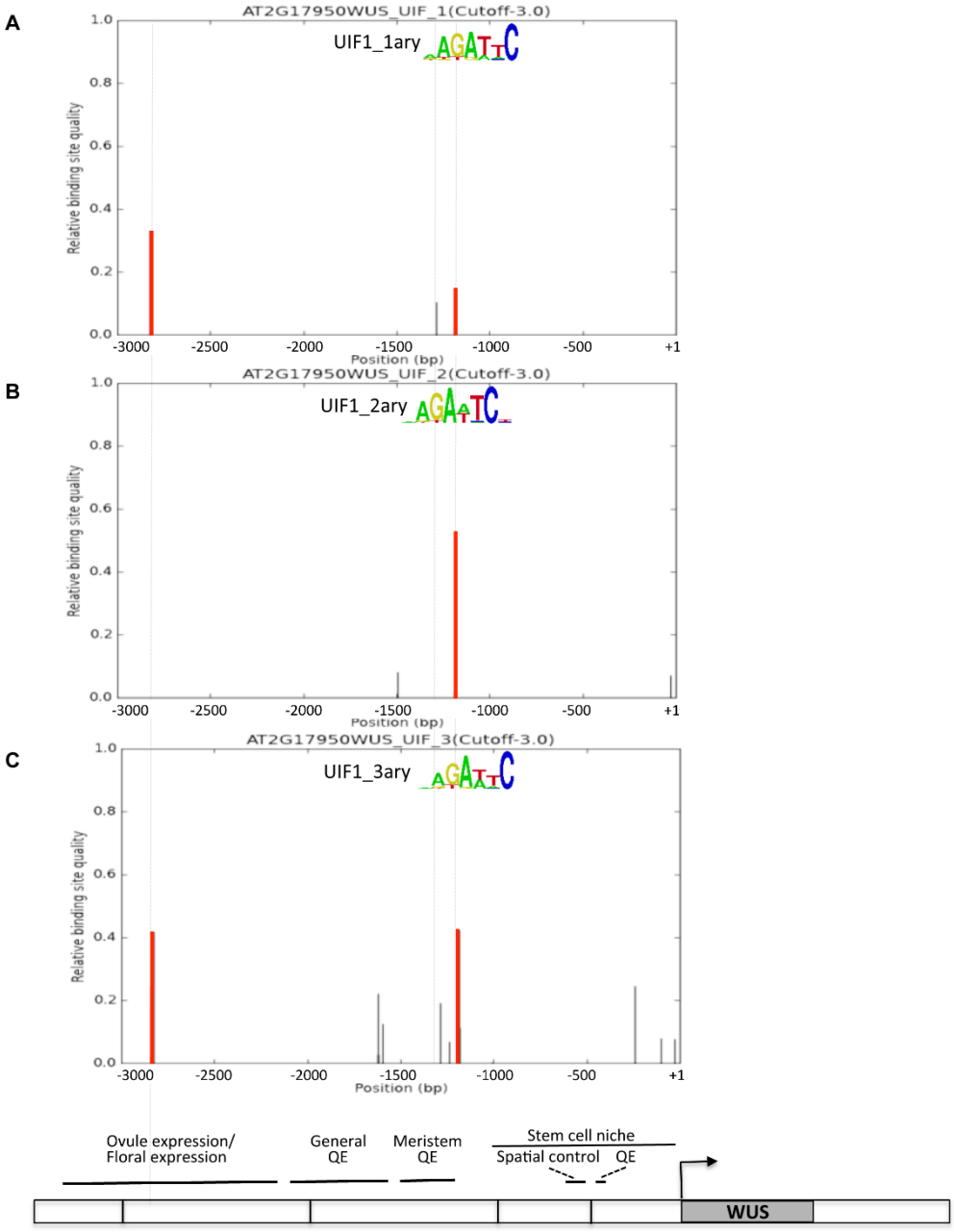

Supplementary Figure S5. Morpheus analysis result on *WUS* promoter sequence. *WUS* promoter sequences were submitted to analyses through the Morpheus program (http://biodev.cea.fr/morpheus/) to predict the probability of potential UIF1 binding sites using UIF1_1ary (A), UIF1_2ary (B) and UIF1_3ary (C) matrices, with a cut-off score of -3. The two best UIF1 binding sites motifs in *WUS* promoter are represented by a red bar *and correspond to* GTAGATTCCT (*WUS-1*: score -1.73107) *and TAGAATATTT* (*WUS-2*: score -1.74376) motifs (position refers to *Baurle and Laux, 2005; WUS promoter elements are indicated at the bottom)*. Other UIF1 binding sites, with a negative score lower than -2, are represented by black bars.

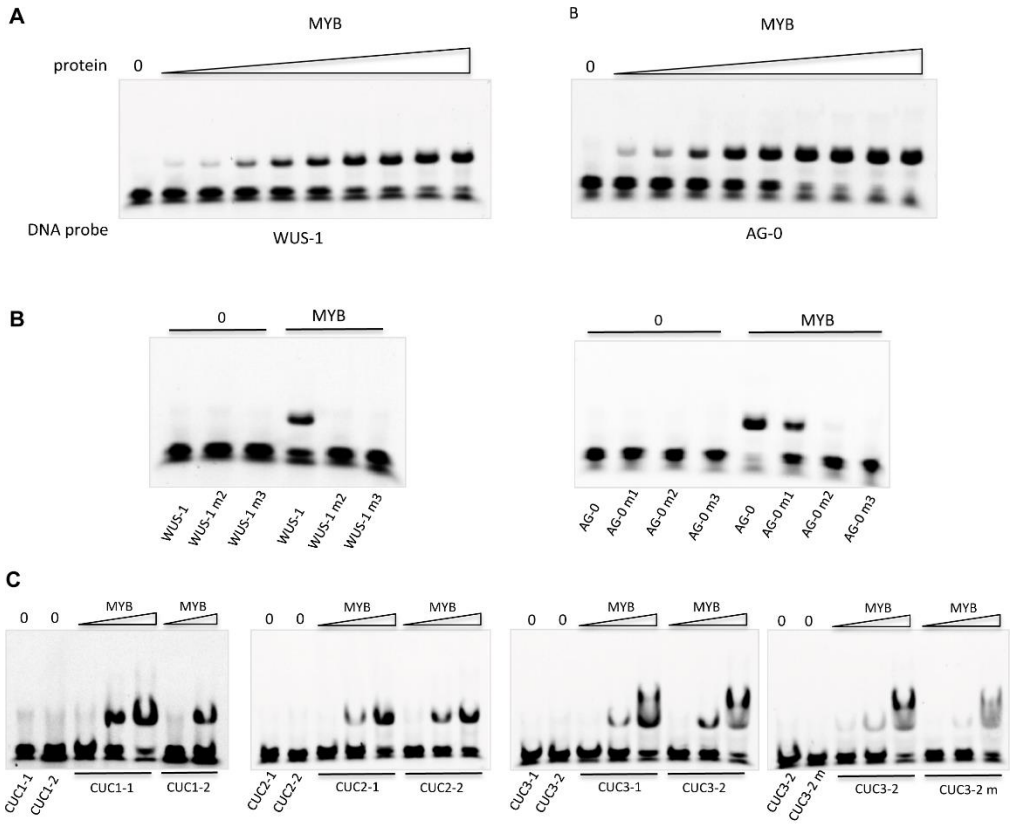

D

Gene	Binding site	Position^{ATG}	oligonucleotides
WUS-1	GTAGATTCCT	- 1182	oETH1433 / oETH1434
mutant m1	GTAGcTTCCT		oETH1466 / oETH1467
mutant m2	GTAGtTTCCT		oETH1491 / oETH1492
mutant m3	GTAGATTgCT		oETH1493 / oETH1494
AG-0	AAGAATCTTT	1922	oETH1435 / oETH1436
mutant m1	AAGcATCTTT		oETH1495 / oETH1496
mutant m2	AAGAATgTTT		oETH1497 / oETH1498
mutant m3	AAGcATgTTT		oETH1504 / oETH1505
CUC1-1	ATGATTCTCT	-1245	oETH1437 / oETH1438
CUC1-2	GTAGAATCCC	- 335	oETH1439 / oETH1440
CUC2-1	AAAGATACAA	- 616	oETH1445 / oETH1446
CUC2-2	ACAGATTCCT	- 333	oETH1447 / oETH1448
CUC3-1	CTGATTCTTT	-1677	oETH1462 / oETH1463
CUC3-2	ATAGAATCAA	-1344	oETH1464 / oETH1465
mutant m	ATAGtATCAA		oETH1501 / oETH1502

Supplementary Figure S6. Electrophoretic mobility shift assay (EMSA). (A-B) The binding properties of UIF1 *MYB* domain (*6*His-*GST*-UIF1-Myb) were tested for binding sites identified in *WUS* and *AG*, (A) using *a gradient of protein concentration (0;* 4 nM; 7.8 nM; 15.6 nM; 31.3 nM; 62.5 nM; 125 nM; 250 nM; 500 nM; 1000 nM) or (B) mutant versions of identified binding sites. In (B), 125 nM of recombinant protein were used. (C) The binding properties of UIF1 *MYB* domain (*6*His-*GST*-UIF1-Myb) were tested for binding sites identified in the *CUC* genes, using *a gradient of protein concentration (*15.6 nM;125nM;1000nM) or mutant versions of identified binding sites. (D) Information on the binding sites and corresponding oligonucleotides used for the EMSA assays.

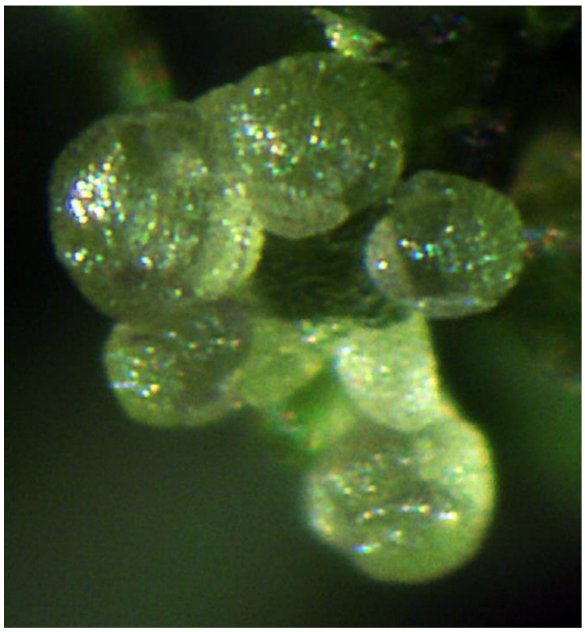

Supplementary Figure S7. Type of dissected inflorescence used in the RT-qPCR experiment shown in Figure 5D. Picture, taken under a dissecting microscope, of a Col-0 inflorescence after removal of flower primordia older than stage 5.

Table S1. List of oligonucleotides used in this study and referred to in the methods.

Purpose	Primer name	Sequence 5'-3'
***uif1* T-DNA lines genotyping**	oUIF1-ADNT06-F	AACATGCAAATCTCGTGGAAG
	oUIF1-ADNT06-R	TGATGCTCTTCATAGGCTTGG
	oLB2	GATATAATAGGAAGC
	oUIF1-ADNT32-F	CATACACGGTTATGCCCATTC
	oUIF1-ADNT32-R	GATCCTCGACACTTCATCGAG
	oLBb1.3	GTTCCGAAATCGGCAAAAT
RT-PCR and RT-qPCR	oUIF1_cDNA_F1	ATGGTTCAAACAGAAACCG
	oUIF1_cDNA_F2	GCTCTTCATAGGCTTGGAGGGCC
	oUIF1_cDNA_R2	GGCCCTCCAAGCCTATGAAGAGC
	oUIF1_cDNA_R1	TCAAAGCTCAAGATCC
	oWUS_cDNA_F	GCAAGCTCAGGTACTGAATGTGGTG
	oWUS_cDNA_R	GACCAAACAGAGGCTTTGCTCTATCG
BiFC	oUIF1sall.F	GTCGACATGGTTCAAACAGAAACCG
	oUIF1-BamH1.R	GGATCCTCAAAGCTCAAGATCC
	oUIF1-BamH1nostop.R	GGATCCCAAAGCTCAAGATCC
	oULT1 sall.F	GTCGACATGGCGAACAATGAGGGAGAGATGC
	oULT1-BamH1.R	GGATCCTCAAGCTTTGACATTGCT
	oULT1-BamH1nostop.R	GGATCCAGCTTTGACATTGCT
	oUIF1dNTsall.F	GTCGACTTATGGCATCTAATGGG
	oULT1dBbCTBamHI.R	GGATCCTCACACCTTCCTGCTCCCTC
	oULT1dBbCT-nostopBamHI.R	GGATCCCACCTTCCTGCTCCCTC
DLRA	oUIF_FAscI	GGCGCGCCGTTCAAACAGAAACCGATC
	oUIF_RXbaI	TCTAGATTAAAGCTCAAGATCCAACACTTG
	oUIF_RdEARXbaI	TCTAGATTACACTTGTCTCTTCTTCTTTGTTTC
	oUIF-ANANA_FAscI	GGCGCGCCGTTCAAACAGAAACCGATCAAAGGATGGGTGCG AAT GCG AATGCG TCTATCT
Subcellular localisation	oUIF1-EcoR1.F	GAATTCATGGTTCAAACAGAAACCG
	oUIF1-BamH1nostop.R	GGATCCCAAAGCTCAAGATCC
	oUIF1-BamH1.R	GGATCCTCAAAGCTCAAGATCC
RNA *in situ* hybridization	oISH_UIF_F1	ACCGATCAAAGGATGGGTCT
	oISH_UIF_R1	TAATACGACTCACTATAGGGTCAGTTTCCGGTTTTGCCCT
	oT7 promoter.R	TAATACGACTCACTATAGGG
Bacteria expression constructs	oETH1239	TACCATGGTTCAAACAGAAACC
	oETH1416	CCATGGCACAGAAGAAAGAGCAG
Yeast expression constructs	oETH1368	CCATTCGAATTCATGGTTCAAACAGAAACC
	oETH1369	GAATGGGGATCCTCAAAGCTCAAGATCCAA
	oETH1381	TATGCTGAATTCATGGCGAACAATGAGGGA
	oETH1382	GCAGCAGGATCCTCACCTGCTCCCTCTCTC
	oETH1410	GAATTCATGGCATCCATGTTGTTT
	oETH1411	GGATCCTCACTTCTTTGATGATTC
	oETH1383	TATCAAGAATTCATGGCGAACAATGAGGGA
	oETH1384	TCACTAGGATCCTCACCTGCTCCCTCTCTC
	oETH1490	GAATTCATGGTTCAAACAGAAACC
	oETH1240	ATCTCGAGTCAAAGCTCAAGATC

EMSA	*WUS-1*	oETH1433	GTATGAAATTTGTAGATTCCTAAAAAAATCT
		oETH1434	AGATTTTTTTAGGAATCTACAAATTTCATA
	AG-0	oETH1435	GGTCTTTGTTAAAGAATCTTTGATCACGTCA
		oETH1436	TGACGTGATCAAAGATTCTTTAACAAAGAC
	CUC1-1	oETH1437	GGTCGGCGGAGATGATTCTCTCATCCACCAC
		oETH1438	GTGGTGGATGAGAGAATCATCTCCGCCGAC
	CUC1-2	oETH1439	GTTAGGCTGACGTAGAATCCCCTGAATTTCA
		oETH1440	TGAAATTCAGGGGATTCTACGTCAGCCTAA
	CUC2-1	oETH1445	GAGATAAAAAAAAAGATACAATCTGAATCCT
		oETH1446	AGGATTCAGATTGTATCTTTTTTTTATCT
	CUC2-2	oETH1447	GAGAGAAAACCACAGATTCCTATGAAAGAGT
		oETH1448	ACTCTTTCATAGGAATCTGTGGTTTTCTCT
	CUC3-1	oETH1462	GATCTTTTTACCTGATTCTTTTGTATCATTC
		oETH1463	GAATGATACAAAAGAATCAGGTAAAAAGAT
	CUC3-2	oETH1464	GGAGGAAGAGTATAGAATCAACCGAACCAAC
		oETH1465	GTTGGTTCGGTTGATTCTATACTCTTCCTC
	WUS-1 m1	oETH1466	GTATGAAATTTGTAGCTTCCTAAAAAAATCT
		oETH1467	AGATTTTTTTAGGAAGCTACAAATTTCATA
	WUS-1 m2	oETH1491	GTATGAAATTTGTAGTTTCCTAAAAAAATCT
		oETH1492	AGATTTTTTTAGGAAACTACAAATTTCATA
	WUS-1 m3	oETH1493	GTATGAAATTTGTAGATTGCTAAAAAAATCT
		oETH1494	AGATTTTTTTAGCAATCTACAAATTTCATA
	AG-0 m1	oETH1495	GGTCTTTGTTAAAGCATCTTTGATCACGTCA
		oETH1496	TGACGTGATCAAAGATGCTTTAACAAAGAC
	AG-0 m2	oETH1497	GGTCTTTGTTAAAGAATGTTTGATCACGTCA
		oETH1498	TGACGTGATCAAACATTCTTTAACAAAGAC
	AG-0 m3	oETH1504	GGTCTTTGTTAAAGCATGTTTGATCACGTCA
		oETH1505	TGACGTGATCAAACATGCTTTAACAAAGAC
	CUC3-2 m1	oETH1501	GGAGGAAGAGTATAGTATCAACCGAACCAAC
		oETH1502	GTTGGTTCGGTTGATACTATACTCTTCCTC